piRNAs safeguard splicing and RNA fidelity during heat shock

Sehee Min, Johnny Cruz-Corchado, and Veena Prahlad*

*corresponding author

Veena.prahlad@roswellpark.org 716-845-8086

Department of Cell Stress Biology

Roswell Park Comprehensive Cancer Center

Elm and Carlton Streets

Buffalo, NY 14263

Keywords: piRNA, heat shock, *hsp,* splicing, nonsense-mediated decay (NMD), endo-siRNAs, transcript fidelity, RNA quality control, protein homeostasis, *C. elegans*

ABSTRACT

Piwi-interacting RNAs (piRNAs) silence transposons and foreign sequences; yet, for poorly understood reasons, they also extensively target endogenous mRNAs. Here, we report a previously unappreciated role for the *Caenorhabditis elegans* piRNA pathway in RNA quality control: during heat shock, piRNAs generate endogenous antisense RNAs (endo-siRNAs) that associate with RNA Polymerase II and nascent stress-induced RNAs to delay splicing when the spliceosome is compromised, minimizing transcript errors. In the absence of piRNAs, nascent transcripts undergo premature splicing, accumulate errors, and activate nonsense-mediated decay (NMD) to limit the production of aberrant proteins. We propose that by regulating splicing, the piRNA pathway acts alongside NMD as a quality-control system, safeguarding RNA fidelity and proteome integrity with genome defense.

30 **Introduction**

31 Piwi-interacting RNAs (piRNAs) are small, single-stranded RNA guides for PIWI Argonaute
32 proteins that suppress transposable elements and foreign RNAs through transcriptional and post-
33 transcriptional silencing(*1-10*). Yet, across animal species, a large proportion of piRNAs target
34 endogenous genes, suggesting that the piRNA pathway also plays evolutionarily ancient and
35 conserved roles in regulating gene expression(*1-7, 11-15*). However, their endogenous functions
36 remain mostly unknown. In *Caenorhabditis elegans*, piRNAs associate with PRG-1 (the *C.*
37 *elegans* PIWI protein) and can target, with high mismatch tolerance, nearly all germline RNAs,
38 including ectopic sequences such as GFP transgenes(*1, 2, 16, 17*). piRNA-targeting initiates the
39 production of secondary antisense small endogenous silencing RNAs (endo-siRNAs, or 22G-
40 RNAs) templated from the piRNA-targeted mRNAs by RNA-dependent RNA polymerases
41 (RdRPs)(*18-20*). These 22G-RNAs recruit WAGO Argonaute proteins to enforce co- and post-
42 transcriptional silencing. Self-RNAs are spared this promiscuous silencing through their
43 interactions with another Argonaute protein, CSR-1, guided by 22G-RNAs generated from actively
44 translated transcripts independently of piRNAs(*21, 22*). These CSR-1-associated 22G-RNAs,
45 thus, act as molecular engrams that recognize expressed 'self' genes to prevent their silencing.
46 However, this leaves unexplained how inducible genes— normally absent and thus lacking CSR-
47 1-22G-RNA guides, but whose expression is necessary for organismal function— escape piRNA-
48 mediated silencing.

49

50 To address this question, we conducted RNA-sequencing to profile mRNAs, piRNAs, and 22G-
51 RNAs after subjecting *C. elegans* to heat shock—a stimulus which induces the abrupt and
52 massive expression of heat shock protein (*hsp*) and other mRNAs necessary to survive stress,
53 but which are typically undetectable in unstressed cells (*23-25*). We found that instead of escaping
54 piRNA surveillance, surprisingly, the piRNA system targeted *hsps* and other stress-induced
55 mRNAs, producing robust endo-siRNAs (22G-RNAs) antisense to these transcripts. Therefore,

56 to understand the functional role of this targeting, we investigated the effects of the piRNA/22G-
57 RNA system on nascent transcript synthesis, maturation, turnover, and fidelity, using *hsps* as
58 model transcripts, and 5-ethynyluridine (EU) pulse-chase labeling, Adapted Photoactivatable
59 Ribonucleoside-Enhanced Crosslinking and Immunoprecipitation (PAR-CLIP), chromatin
60 fractionation, and Unique Molecular Identifier- (UMIs)-labelling (*26-30*) to analyze transcript
61 errors. We found that the piRNA system biases splicing decisions, favoring post- rather than co-
62 transcriptional splicing. This restrains splicing during heat shock when the spliceosome is
63 compromised, increasing the pool of unspliced pre-mRNA to be processed during stress recovery,
64 and limiting transcript errors. We show that the piRNA-generated 22G-RNAs enforce splicing
65 delays by interacting with Pol II and nascent RNA, promoting chromatin retention of mature
66 transcripts. In contrast, in the absence of piRNAs and associated 22G-RNAs, splicing is
67 accelerated, resulting in genome-wide misregulation of long, intron-rich genes, the accumulation
68 of transcript errors, and the increased activation of the nonsense-mediated decay (NMD) pathway
69 to prevent protein misfolding and ensure survival. Based on these studies, we propose that the
70 pervasive targeting of endogenous genes by the piRNA system serves a previously unrecognized
71 but critical role in RNA quality control.
72

73 **Results**

74 **Heat-shock induced *hsp* and other mRNAs are targeted by the piRNA pathway**

75 To understand the role of the piRNA system in regulating inducible genes, we performed small
76 RNA (sRNA-seq) and mRNA (paired-end, strand-specific, polyA-selected) sequencing from
77 synchronized day-one adults exposed to mild (5 mins, 34°C) or strong (30 mins, 34°C) heat shock
78 (Suppl. Fig 1a; Suppl. Tables 1, 2). Animals were also analyzed after two hours of recovery at
79 20°C, when normal physiological functions largely resume(*31*). In parallel, to identify piRNA-
80 dependent effects, we sequenced *prde-1* mutants, deficient in piRNA biogenesis(*32, 33*) (Suppl.
81 Fig. 1a; Suppl. Tables 1, 2). As expected, heat shock induced global changes in mRNA (Suppl.

82 Fig 1b), including the massive upregulation of *hsp* genes (Fig 1a; Suppl. Fig 1c, d *mRNA*).
83 Surprisingly, in wild-type animals, heat shock also produced 22G-RNAs antisense to the *hsp*
84 mRNAs (Fig 1a; Suppl. Fig 1c, d *22G-RNA*), suggesting that rather than escaping piRNA
85 surveillance, *hsp* mRNAs may be targeted by the piRNA system. Like the *hsp* mRNAs, these
86 antisense 22G-RNAs also appeared within 5 minutes of heat shock and peaked during recovery
87 (Fig 1a; Suppl. Fig 1c, d *22G-RNA*). Consistently, by 30 minutes of heat shock, several piRNAs
88 were also modestly but significantly induced (Suppl. Fig 1e, f). In *prde-1* mutants, *hsp* induction
89 upon heat shock appeared unperturbed, but many fewer 22G-RNAs antisense to *hsp* mRNAs
90 were produced (Fig 1a; Suppl. Fig 1c, d *mRNA; 22G-RNA*), indicating that these 22G-RNAs were
91 generated because of piRNA-targeting.
92
93 Because piRNA targeting of mRNAs generates 22G-RNAs through the activities of the PIWI
94 Argonaute PRG-1 and RdRPs that reside in perinuclear condensates (nuage or germ granules)
95 of the germline(*16, 19*), to confirm these unexpected results, we tested whether *hsp* mRNAs
96 interact with PRG-1. (*34, 35*). First, we determined whether *hsps* are also induced in the germline
97 upon heat shock, by conducting RNA Fluorescence *in situ* hybridization (RNA FISH; Fig 1b, c;
98 Suppl. Fig 2a) to localize *hsp-70s (C12C8.1* and *F44E5.4/.5)*. Heat shock induced the expression
99 of *hsp-70* mRNAs in the late pachytene nuclei (and only these nuclei) of the germline. Moreover,
100 although PRG-1 localization is known to dissolve upon exposure to increased temperatures and
101 indeed does so in regions such as the transition zone (TZ; Fig 1d), PRG-1 remained in perinuclear
102 condensates upon heat shock in the pachytene nuclei (Fig. 1d; compare transition zone, TZ,
103 where *hsp* mRNAs are absent, with Pachytene), supporting potential *hsp-70*-PRG-1 interactions.
104 Next, we immunoprecipitated PRG-1 under control, heat-shock, and recovery conditions from
105 animals expressing FLAG-tagged PRG-1 to determine whether *hsp-70 (C12C8.1* and *F44E5.4/.5)*
106 mRNAs associated with PRG-1 (native RNA immunoprecipitation, RIP, followed by RT–qPCR;
107 Fig 1e, f). Non-FLAG animals were used to account for non-specific interactions of *hsp* mRNAs,

108 and *bath-45,* a known piRNA target, served as a positive control (Fig 1e, f; Suppl. Fig 2b). These
109 experiments also indicated that *hsp-70s* interacted with PRG-1 upon heat shock, and *hsp-70*
110 *(C12C8.1)*, but not *hsp-70 (F44E5.4/.5)* remained associated for a longer duration, even during
111 recovery (Fig 1e, f; Suppl. Fig 2b). Finally, and most convincing, we depleted PRDE-1 specifically
112 in the germline using an auxin-inducible degron (AID) system, and found that this abolished 22G-
113 RNAs presence throughout the animal (RNA FISH), demonstrating that 22G-RNAs originate in
114 the germline through piRNA targeting (Fig 1g, h; embryos show non-specific staining).
115 Surprisingly, despite their germline origin, the 22G-RNAs were present throughout the animal, in
116 somatic cells that expressed *hsp* mRNA (e.g. muscle, somatic sheath cells), as well as in the
117 germline cells such as sperm, which do not (RNA FISH; Fig 1g, h; Suppl. Fig 2c). Upon germline
118 depletion of PRDE-1, 22G-RNA levels were starkly decreased in somatic and germline cells (Fig
119 1g, h), while *hsp-70* mRNA continued to be expressed (Suppl. Fig 2c). Together, these findings
120 confirmed that *hsp* mRNAs were subject to piRNA surveillance, actively targeted by the canonical
121 piRNA pathway in the germline, and produced 22G-RNAs that propagated systemically across
122 tissues.
123
124 Further evidence that the *hsp* genes induced by heat shock were templating antisense 22G-RNA
125 production came from profiling mRNAs and sRNAs in a mutant in heat shock factor 1 (HSF1;
126 HSF-1 in *C. elegans*), the transcription factor responsible for *hsp* expression upon heat shock.
127 This mutant, *hsf-1 (sy441)* is deficient in heat-induced activity but expresses higher basal levels
128 of *hsp* mRNA(*31, 36*). Yet *hsf-1* mutants failed to produce 22G-RNAs antisense to *hsp* genes (Fig
129 1a; Suppl. Fig 1c, d). Surprisingly, even the few *hsp* mRNAs, like *hsp-70 (F44E5.4/.5)*, that did
130 accumulate upon heat shock in *hsf-1 (sy441)* mutants, did not template 22G-RNAs (Suppl. Fig
131 1c, d), perhaps suggesting a broader role for HSF-1 in piRNA-dependent 22G-RNA production.
132

133 piRNA surveillance was not limited to *hsps*, but extended to other heat-shock-regulated genes:
134 ~15% of differentially expressed genes (DEGs) upon a 5-minute heat-shock and ~40% by 30
135 minutes templated 22G-RNA production, and both the numbers of DEGs, and DEG-derived 22G-
136 RNAs were reduced in *prde-1* and *hsf-1* mutants (Fig 1i; Suppl. Fig 2d; Suppl. Table 3). 22G-RNA
137 function is determined by its Argonaute partner; however, the 22G-RNAs that targeted *hsp*
138 mRNAs were 'unclassified' and not previously identified in association with known *C. elegans*
139 Argonaute proteins (Suppl. Fig 3; Suppl. Table 4). However, other DEGs did template 22G-RNAs
140 that had been previously identified as guide RNAs for WAGO, CSR-1, and other Argonaute
141 proteins (Suppl. Table 4). WAGO-associated 22G-RNAs that were induced upon 30 minutes of
142 heat shock exposure were piRNA-dependent, as apparent by their decreased levels in *prde-1*
143 mutants, and in wild-type they increased as their target mRNAs decreased, consistent with their
144 known roles in post-transcriptional or co-transcriptional silencing(*8, 37*) (Suppl. Fig 3a, b). CSR-
145 1 22G-RNAs declined upon heat shock (perhaps due to translational attenuation), as their target
146 mRNAs rose in both wild type and *prde-1* mutants, consistent with their mostly piRNA-
147 independent production (Suppl. Fig 3a, b). Unclassified 22G-RNAs, meaning those whose
148 Argonaute partners had not been previously identified, continued to increase in a *hsf-1-* and *prde-*
149 *1-* dependent manner, even during recovery from heat shock, as did their complementary mRNAs
150 (Suppl. Fig 3a, b). The effects were dynamic and reversible during recovery from stress (Suppl.
151 Fig 2d (Rec); Suppl. Fig 3a, b), and the mRNAs that templated 22G-RNA production showed
152 distinct GO enrichments (Suppl. Fig 4; Suppl. Table 5).
153
154 Together, these results suggested that the broad piRNA-dependent and independent 22G-RNA
155 expression that was triggered by heat shock likely contributes to the pervasive transcriptome-
156 wide remodeling(*8, 37*) universally associated with this stress-induced transcription program.
157
158 **The piRNA-pathway regulates post-transcriptional splicing.**

159 Given the known roles of piRNAs in post- and co-transcriptional silencing, we suspected that
160 piRNA targeting of *hsp* and other stress-induced genes functioned to clear transcripts during
161 recovery from heat shock. If so, *hsp* mRNAs should persist longer after stress in *prde-1* mutants.
162 Instead, RT-qPCR (Suppl. Fig 5a-c) and RNA-FISH (Suppl. Fig 5d) revealed the opposite: the
163 steady state abundance of *hsp* mRNAs declined more rapidly in *prde-1* mutants compared to wild
164 type. We examined whether decreased RNA Polymerase II (Pol II) binding at *hsp* genes(*38*), or
165 altered transcription duration, explained this progressive decline. But this was also not the case:
166 chromatin immunoprecipitation followed by qPCR (ChIP-qPCR) showed that Pol II levels at *hsp*
167 gene transcription start sites (TSS), and its return to basal levels by 2 hours post-heat shock,
168 were similar in *prde-1* and wild-type animals (Suppl. Fig 5e, f). Therefore, to understand the role
169 of the piRNA pathway's targeting of *hsps* and other heat-shock genes, we directly assessed *hsp*
170 mRNA dynamics in the absence and presence of the piRNA pathway by tracking their synthesis
171 and turnover using a pulse-chase metabolic labeling approach: i.e., we labeled the heat-shock
172 induced pre-mRNA with 5-ethynyluridine (EU)(*39, 40*) provided to the animals only during heat
173 shock exposure, and tracked the fate of this RNA by absolute RT–qPCR using exon–intron (pre-
174 mRNA) and exon–exon (mature mRNA) primers during recovery from heat shock (Fig 2a; see
175 methods for experimental details).
176
177 These studies revealed that in the absence of piRNAs, *hsp* splicing or maturation occurred at an
178 accelerated pace, resulting in a precocious increase in nascent mRNAs and a concomitant
179 decrease in pre-mRNA pools, whereas the presence of piRNAs in wild-type animals restrained
180 splicing. The evidence for this was as follows. First, consistent with similar Pol II occupancy at
181 *hsp* genes, *prde-1* synthesized similar total amounts of RNA as wild-type animals upon heat shock
182 (Suppl. Fig 5g, h). Despite this, *prde-1* mutants had significantly reduced amounts of nascent (EU-
183 labeled) pre-mRNA by the end of the 30-minute heat shock (Fig 2b; Suppl. Fig 5i), but, on the
184 other hand, accumulated significantly more EU-containing spliced mRNA by 2 hours following

185 heat shock (Fig 2c; Suppl. Fig 5j). Next, the amounts of unspliced nascent pre-mRNA present at
186 the end of heat shock exposure, calculated as the ratio of EU-labeled pre-mRNA over total EU-
187 labeled RNA(*41*), was higher in wild-type animals expressing piRNAs/22G-RNAs compared to
188 *prde-1*: ~75% of nascent *hsp-70 (C12C8.1)* transcripts, which contain two introns, remained as
189 pre-mRNA to be spliced post-transcriptionally during recovery in wild-type animals (Fig 2d),
190 whereas only ~57% persisted unspliced in *prde-1* mutants (Fig 2d). Thus, the piRNA pathway
191 biased the decision between co- and post-transcriptional splicing toward delayed splicing. Finally,
192 this remaining *hsp-70 (C12C8.1)* was also spliced more rapidly in *prde-1* animals: within 2 hours
193 of recovery, dramatically more EU-containing spliced mRNAs were produced from the nascent
194 EU-labeled unspliced pre-mRNA (Fig 2e). The other inducible *hsp-70 (F44E5.4/.5)*, contained
195 only one intron, and was mainly co-transcriptionally spliced in both wild-type and *prde-1* animals
196 (Suppl. Fig 5k). Still, the post-transcriptional splicing of the residual *hsp-70 (F44E5.4/.5)*
197 proceeded markedly faster in *prde-1* mutants than in wild-type animals (Suppl. Fig 5l). This was
198 also true for the small heat shock protein (*hsp-16.11*; Suppl. Fig 5m).
199
200 Besides the co- and/or post-transcriptional splicing of *hsp* mRNAs, the piRNA system appeared
201 to broadly regulate transcriptome-wide splicing decisions: in wild-type animals compared to *prde-*
202 *1* mutants, heat shock-DEGs (p.adj <0.05) expressed more alternatively spliced (AS) isoforms,
203 as indicated by their much lower "percent spliced in" (PSI or Ψ)(*42, 43*) values (Fig 2f). In addition,
204 540 transcripts showed significant dPSI (differential PSI; p <0.1) values, compared to only 139
205 transcripts in *prde-1* (Suppl. Table 6). Moreover, for seven representative AS events(*44, 45*) —
206 retained intron (RI), alternative 5'/3' Splice Sites (A5/A3), skipped exon (SE), mutually exclusive
207 exons (MX), and alternative first and last exons (AF/AL) (Fig 2j) — mRNAs differentially expressed
208 upon heat shock in wild-type animals were significantly less spliced, retaining more introns
209 compared to *prde-1* (Fig 2g; Suppl. Table 7). In further support of the role of the piRNA system in
210 alternative splicing, nearly 40% (125/308) of DEGs that produced AS transcripts upon heat shock

211 in wild-type animals also templated 22G-RNAs, while only 12% (35/280) did so, in *prde-1* (Suppl.
212 Fig 6a). These AS mRNAs were enriched in developmental processes, and in particular for
213 neuronal functions known to rely more on alternative splicing (Suppl. Fig 6b; Suppl. Table 8). This
214 suggested that their delayed splicing may be important for the restoration of developmental
215 processes during recovery from heat shock, and accordingly, heat-shocked *prde-1* mothers
216 showed a marked delay in generating viable embryos post-heat shock (Suppl. Fig 6c, d). These
217 results showed that the piRNA pathway, perhaps by virtue of the sequence complementarity of
218 the 22G-RNAs it produced, impacted transcriptome wide splicing decisions upon heat shock.
219
220 To determine whether the splicing decisions were dynamically controlled by the piRNA system,
221 we investigated whether we could rescue *hsp* RNA dynamics by microinjecting small RNAs
222 obtained from heat-shocked wild-type animals into *prde-1* animals shortly before subjecting them
223 to heat-shock exposure (Fig 2h). This was indeed the case: when *prde-1* animals were
224 microinjected with small RNA fraction (<200nt) obtained from heat-shocked wild-type animals, but
225 not with small RNA fractions from heat-shocked *prde-1* animals, both the persistence of *hsp*
226 mRNA (Fig 2i, j), and the levels of *hsp* pre-mRNA were partially rescued (Fig 2k). Small RNA
227 injections *per* se did not induce or enhance *hsp* expression (Fig 2i, j).
228
229 Thus, together, the results from pulse-chase metabolic labeling, transcriptome-wide alterations in
230 AS, and microinjection rescue experiments suggested that the piRNA/22G-RNA pathway
231 functioned dynamically, to alter splicing decisions to preserve mRNA expression during heat-
232 shock recovery by restraining splicing and maintaining a pool of pre-mRNAs for delayed
233 processing.
234
235 **22G-RNAs act through a 'telescripting'-like mechanism to protect long gene expression.**

236 Mechanistically piRNA/22G-RNAs could regulate splicing indirectly, through their known
237 interactions with chromatin(*8, 34, 46*). Alternatively, and consistent with their ability to rescue *hsp*
238 expression dynamics, and the rapid expression of *hsp* genes that occurs upon heat shock, the
239 piRNA/22G-RNAs could regulate splicing directly by acting on target pre-mRNAs at the
240 transcription complex to bias splicing decisions(*47*). Therefore, to understand how 22G-RNAs
241 regulate splicing, we adapted Photoactivatable Ribonucleoside-Enhanced Crosslinking and
242 Immunoprecipitation (PAR-CLIP) to test whether these small RNAs are associated with Pol II at
243 the transcription complex. In addition, because co-transcriptional splicing occurs during Pol II
244 elongation, but the mechanisms that regulate the timing, transition, and completion of post-
245 transcriptional splicing are still unclear(*48, 49*), we immunoprecipitated Pol II immediately at 30
246 minutes upon heat shock, when transcription was still in process, or after 2 hours of recovery from
247 heat shock, when Pol II was no longer engaged with the *hsp* locus (ChIP-qPCR; Suppl. Fig 5e,
248 f), but spliced mRNAs accumulated in cells (Fig 2c; Suppl. Fig 5j), and determined the levels of
249 nascent *hsp* mRNA or pre-mRNA that remained associated with Pol II along with the 22G-RNAs.
250
251 Animals were fed 4-thiouridine (4sU) at non-inhibitory concentrations (Fig 3a; Suppl. Fig 7a, b),
252 subjected to heat shock, exposed to UV (365 nm) to crosslink nascent 4sU-containing RNA to Pol
253 II at the described time points, Pol II was immunoprecipitated, and the RNA species associated
254 with Pol II identified using absolute and stem-loop RT-qPCR. In wild-type animals, as expected,
255 unspliced *hsp* pre-mRNAs co-immunoprecipitated with Pol II at 30 minutes after heat shock,
256 decreasing by 2 hours post-heat shock recovery (Fig 3b; Suppl. Fig 7d). Nevertheless, a small
257 but significant fraction of nascent pre-mRNA remained associated with Pol II 2 hours post-heat
258 shock (Fig 3b; Suppl. Fig 7d), when Pol II was no longer transcriptionally engaged (ChIP-qPCR;
259 Suppl. Fig 5e, f). Notably, 22G-RNAs antisense to *hsp-70* (*C12C8.1*) also co-immunoprecipitated
260 with Pol II, 2 hours post-heat shock (Fig 3c), as concomitantly, increasing amounts of *hsp-70*
261 mRNA were spliced, and also associated with Pol II (Fig 3d). Furthermore, chromatin fractionation

262 showed that these progressively increasing spliced mRNAs were retained in chromatin (Fig 3e,
263 f). In *prde-1* mutants, less pre-mRNA (Fig 3b), but more constitutively spliced nascent mRNA (Fig
264 3d) was associated with Pol II at 30 minutes heat shock, and 22G-RNAs were not present (Fig
265 3c). In addition, spliced *hsp-70* mRNA failed to increase on chromatin (Fig 3e, f), or in association
266 with Pol II above these basal constitutive levels (Fig 3d), instead appearing to be efficiently
267 exported and translated as seen by elevated HSP-70 protein levels (Fig 3g).
268
269 A broadly similar dynamic was observed with *hsp-70 (F44E5.4/.5)*, even though the majority of
270 RNA was spliced co-transcriptionally (Suppl. Fig 5k). Here, by the end of 30 minutes of heat shock,
271 the remaining amounts of pre-mRNA that associated with Pol II were similar in wild-type and *prde-*
272 *1* animals (Suppl. Fig 7d), but significantly more mRNA was crosslinked with Pol II in wild-type
273 animals (Suppl. Fig 7e), remained associated with Pol II during recovery (Suppl. Fig 7e), and
274 accumulated in chromatin (Suppl. Fig 7f). Also, like with *hsp-70 (C12C8.1)*, significantly more
275 22G-RNA associated with Pol II in wild-type animals compared to *prde-1* (Suppl. Fig 7g). Perhaps
276 due to the difference in splicing strategy between the two *hsp-70s*, 22G-RNA kinetics in
277 association with Pol II varied: at 30 minutes upon heat shock, 22G-RNA associated with Pol II
278 decreased in *prde-1*, rather than increasing in wild-type. Notwithstanding these differences, these
279 data together showed that the piRNA-generated 22G-RNAs act at the transcription complex,
280 associating with Pol II, to delay splicing, and promote chromatin retention of *hsp* mRNAs,
281 postponing the availability of *hsp-70* mRNAs for translation. The continued association of
282 unspliced and spliced RNAs along with 22G-RNAs with Pol II after transcription was complete
283 and Pol II had disengaged from the *hsp* genes — most evident in *hsp-70 (C12C8.1)*, where a
284 larger fraction underwent post-transcriptional splicing — also suggested that post-transcriptional
285 splicing of *hsp* RNA occurs in direct or indirect association with Pol II.
286

287 The ability of antisense 22G-RNAs to retard splicing at the transcription complex through
288 association with Pol II and nascent pre-mRNA was reminiscent of mechanisms by which U1
289 snRNA base-pairs with nascent transcripts to modulate their splicing efficiency and rates, and
290 initiates telescripting, a process that prevents premature transcription termination, particularly of
291 long-intron containing genes(*50-52*). In mammalian cells, heat shock decreases U1 snRNA levels,
292 resulting in the loss of telescripting and a decrease in the expression of long-intron-containing
293 genes(*53, 54*). Like mammalian cells, *C. elegans*, also showed a modest but significant decrease
294 in at least three of five U1 snRNAs tested (Fig 3h; Suppl. Fig 7h). Yet, unlike mammalian cells, in
295 wild-type *C. elegans,* despite reduced U1 RNA levels, genes upregulated upon heat shock were
296 preferentially enriched for long-intron-containing genes. This was visible in the increase in their
297 average gene lengths (Fig 3i) and the cumulative distribution plots of gene lengths of differentially
298 upregulated and downregulated genes (p.adj <0.05) (Suppl. Fig 8a), and metagene profiles of
299 expression values of all expressed genes segregated by gene length (Suppl. Fig 8b, c; Suppl.
300 Table 9). *prde-1* animals showed a marked deficiency in upregulating long genes, although they
301 did not differ from wild-type in downregulation of long genes (Fig. 3i, Suppl. Fig 8a; also see Suppl.
302 Fig 8b, c). This raised the intriguing possibility that the 22G-RNAs generated by wild-type animals
303 were functionally substituting for U1 snRNAs during stress, ensuring productive Pol II elongation
304 and expression of long-intron-containing genes. In support of this, ChIP–qPCR showed that
305 elongating Pol II (S2P) levels were markedly and significantly decreased at *hsps (C12C8.1* and
306 *F44E5.4/.5)* 3′ ends in *prde-1*, despite normal occupancy at the 5′-end, mirroring phenotypes
307 caused by disrupting U1–nascent RNA interactions(*51, 52*) (Fig 3j; Suppl. Fig 8d).
308
309 Together, these findings indicate that the piRNA pathway delays splicing and promotes chromatin
310 retention of mature mRNAs by associating with the transcription complex. In doing so, the
311 antisense 22G-RNAs act in a manner strikingly similar to U1 during telescripting: both systems

312 protect splicing, preserve Pol II elongation, and the expression of long-intron containing genes,
313 essential for development.
314
315 **The piRNA pathway preserves transcript fidelity and complements nonsense-mediated**
316 **decay as a mechanism enforcing RNA quality control.**
317 The accelerated splicing observed in *prde-1* mutants, even under heat shock conditions when
318 spliceosome function is challenged, and reduced RNA polymerase II occupancy at the 3′ ends of
319 *hsp* genes (Fig 3j, Suppl. Fig 8d), suggested to us that in the absence of piRNAs, mRNA
320 transcripts may be accumulating errors due to aberrant splicing or premature termination. To
321 directly test this hypothesis, we used Unique Molecular Identifiers (UMIs)(*26-30*) to label individual
322 mRNAs from heat-shocked wild-type and *prde-1* mutants during first-strand cDNA synthesis, prior
323 to PCR amplification and library preparation, and subjected these UMI-labeled mRNAs to RNA-
324 sequencing. Following sequencing, we derived consensus mRNA sequences from grouped UMI-
325 labeled mRNAs, which allowed us to differentiate random PCR-generated errors from errors
326 within the original mRNA molecule, mapped these sequences onto the *C. elegans* reference
327 genome, excluded values that could be attributed to potential germline SNPs (see Methods for
328 details), and identified regions of mismatch, reflecting transcript variants or 'errors' (Suppl. Fig 9a;
329 Suppl. Online Material)**.** We then quantified the error rate in the consensus RNA molecules**,** from
330 protein coding genes, or other genomic regions in wild-type and *prde-1* mutants, using two
331 methods: (i) we generated a 'pileup' of all consensus sequences aligned to the reference genome
332 and identified the percentage of nucleotides at each genomic position which were mismatched,
333 and (ii) as a more stringent method, we identified high quality variant containing sites using the
334 program HaplotypeCaller in the Genome Analysis Toolkit (GATK), and selected those annotated
335 by SnpEff with a predicted impact of "High", "Moderate" or "Low" as potential 'errors'. To increase
336 our confidence that any mismatches were 'errors', in both methods, we further selected regions
337 with a minimum coverage of > 10 reads (Suppl. Fig 9a; Suppl. Online Material). Generating a

338 pileup from the aligned mRNAs allowed us to approximate a mean error rate across all nucleotides
339 (Global error rate) during heat shock as being in the order of approximately 10-3/bp, and compare
340 the distribution of error-prone mRNA sequences between *prde-1* and wild-type. This differed
341 significantly (Kolmogorov-Smirnov (KS) test; p<2e -16; Suppl. Table 10), with mRNA from the
342 *prde-1* animals displaying a higher mean error rate than wild-type (Fig 4a) and expressing error-
343 prone mRNAs enriched for distinct biological processes (Fig 4b; Suppl. Table 11, 12). *prde-1*
344 mutants also displayed an increased error rate when variants were called more stringently using
345 HaplotypeCaller (Fig 4c, Suppl. Fig 9b, c; Suppl. Table 13). Here, 1315-1684 nucleotide positions
346 in the approximately 3.7×10^7 individual mRNAs per sample analyzed were identified as high-
347 quality variant-sites, and a significantly larger fraction of mRNA molecules that were differentially
348 upregulated in *prde-1* mutants compared to wild-type, under either control or heat shock
349 conditions, harbored these variants (Fig 4c; p.adj <0.05; Suppl. Table 13). Notably, the *prde-1*
350 variant mRNAs were not uniformly distributed across the genome; instead, they were
351 disproportionately enriched in mRNAs from smaller genes, which were also more highly
352 expressed by *prde-1* (Suppl. Fig 9c; see Suppl. Fig 8c for expression levels). Amongst the base
353 changes G>A was the most highly represented (Suppl. Fig 9d), consistent with the increased error
354 rates associated with misincorporation of faster-incorporating bases by Pol II(*55*). This suggested
355 that the splicing delay imposed by the piRNA pathway protected transcript fidelity under stress,
356 and in its absence, animals may be accumulating more 'errors' in their transcripts. However, this
357 analysis did not exclude the possibility that these variants represented RNA modifications or
358 increased RNA-editing in the *prde-1* animals.
359
360 Therefore, to independently evaluate whether *prde-1* animals accumulated more splicing errors,
361 we examined whether these animals have upregulated the nonsense-mediated mRNA decay
362 (NMD) pathway, a system that surveils and eliminates transcripts that are unproductively
363 spliced(*56-61*). If this were the case, we expected known mRNAs that are constitutive NMD

364 targets to be expressed at higher levels upon downregulating *smg-1*, the NMD kinase, or *smg-2*
365 (homolog of UPF1)(*62*). Amongst five previously characterized, reliable NMD targets in *C.*
366 *elegans* (61), four were upregulated more in *prde-1* than in wild type animals upon downregulating
367 *smg-1* or *smg-2* (Fig 4d). This implied that in the absence of piRNA, *prde-1* mutants may be
368 constantly generating unproductively spliced mRNAs, that activated NMD.
369
370 This hypothesis was strongly supported: downregulating *smg-1*, resulted in the complete loss of
371 viability of *prde-1* embryos, not only upon heat shock but also under control conditions (Fig 4e, f).
372 Downregulating *smg-2* and *smg-3* (homolog of UPF2)(*62*) in parents also resulted in complete or
373 partial loss of viability in their embryos, again even under control conditions, or if parents were
374 subjected to heat shock (Fig 4f). In contrast, wild-type embryos were not affected by *smg-1, smg-*
375 *2, smg-3* RNAi, under either heat shock or control conditions (Fig 4e, f), consistent with previous
376 studies showing that NMD is not required for *C. elegans* survival (*56, 62, 63*). Thus, it appeared
377 that the mis-transcribed mRNA in *prde-1* was likely being eliminated during translation to maintain
378 viability. Consistent with this expectation, in the absence of *smg-1*, *prde-1* animals accumulated
379 significantly higher amounts of polyubiquitinated proteins even under control conditions, in the
380 absence of proteotoxic stress (Fig 4g; see methods for how viable *smg-1*-RNAi-treated *prde-1*
381 were obtained).
382
383 Taken together, these studies suggest that piRNAs play a critical role in maintaining RNA integrity,
384 acting as a complementary mode of RNA quality control to NMD: piRNAs delay splicing to
385 preserve accurate pre-mRNAs under stress, while NMD serves to eliminate erroneous transcripts
386 when this buffering mechanism is lost (Fig. 4h).
387
388 **Discussion.**

389 Post-transcriptional control of gene expression is emerging as a critical mechanism to regulate
390 development, stress, and phenotypic plasticity(*47, 48*). Yet how cells select transcripts for delayed
391 splicing, how such delays are mechanistically implemented, and whether and how splicing
392 decisions are coordinated across diverse tissues remain poorly understood. The sequence
393 complementarity of 22G-RNAs to expressed exonic regions of mRNAs, their responsiveness to
394 transcriptional and translational events within the cell, the interactions of 22G-RNAs with nascent
395 transcript and Pol II after Pol II has dissociated from its target gene, and the ability of small RNAs
396 to cross cell boundaries might allow the piRNA/22G-RNAs to act as flexible and systemic
397 modulators of post-transcriptional splicing decisions. While we are yet to identify the detailed
398 mechanisms of splicing regulation, the similarities to U1 RNA-mediated splicing and
399 telescripting(*50-54*) are striking: both systems use base-pairing of noncoding RNAs to stabilize
400 nascent transcripts, bias splicing, stabilize pre-mRNAs, prevent the premature loss of elongating
401 Pol II from the 3' end of genes, and protect the expression of long-intron-containing genes. These
402 parallels raise the intriguing possibility that, analogous to therapeutic antisense oligonucleotides
403 under clinical investigation, *C. elegans* may employ piRNA/22G RNAs as a natural small RNA–
404 guided telescripting system to substitute for, or complement, U1 RNAs in RNA splicing.
405
406 Only very few previous studies have linked the piRNA pathway to splicing regulation(*64, 65*). Yet,
407 these studies suggest that the piRNA-splicing-regulation may be conserved across species. Thus,
408 in *Drosophila*(*64*) nuclear Piwi complexes inhibit splicing of the *gypsy* retrotransposon through
409 chromatin-based, co-transcriptional silencing, whereas in locusts(*65*) piRNAs facilitate splicing of
410 specific pre-mRNAs during oocyte maturation, suggesting both inhibitory and stimulating role for
411 piRNAs in splicing control. Intriguingly, in *C. elegans*, the presence of introns protects transcripts
412 from default Argonaute-mediated silencing in the germline, and the WAGO Argonaute, HRDE-1
413 have been shown to interact with the conserved RNA helicase Aquarius/EMB-4(*66-68*), further
414 implicating piRNA function in RNA splicing regulation.

415 What might be the rationale for this unexpected role of piRNAs in splicing observed in our studies?
416 piRNAs were initially discovered in germline cells, where they suppress transposons in many
417 animal species. In this context, it is intriguing to note that spliceosomal introns themselves are
418 considered to have evolved from Type II transposons(*69, 70*), opening the tantalizing possibility
419 that the regulation of splicing a possible ancient, and vestigial function of piRNAs. Still, across
420 species, piRNA and their associated PIWI proteins play broad roles in regulating gene expression
421 in both somatic and germline cells, distinguishing self-RNAs from non-self-RNAs like transgenes
422 and retroviral sequences, directing these 'non-self' transcripts for post-transcriptional gene
423 silencing and degradation, directing epigenetic programming, DNA rearrangements, mRNA
424 turnover and translational control (*4, 6, 8, 10, 34, 35, 71-80*). Our studies suggest that the role of
425 piRNAs in regulating splicing and protecting transcript fidelity, while also interacting with the NMD
426 machinery, may be central to these different roles, allowing the piRNA pathway to determine which
427 newly synthesized transcripts are permitted sustained expression. piRNAs are amongst the
428 fastest evolving small RNAs (*4, 6*). Likewise, AS is among the most divergent modes of gene
429 expression and has been described as a form of 'evolutionary tinkering'(*44, 81-84*). Indeed, it is
430 thought that AS most likely evolved as an inevitable consequence of splicing errors and was later
431 selected to result in the structural and functional diversification of proteins(*44, 81-84*).
432
433 In *C. elegans*, loss of the piRNA pathway leads to a sporadic, and temperature-dependent
434 increase in infertility over time, a defect that can be mitigated by slowing growth or metabolism(*9,*
435 *85*). In addition, NMD, which mainly silences pseudogenes, is crucial for longevity(*86, 87*). Our
436 findings suggest that similar to aging-dependent neurodegenerative disorders, the increased
437 infertility upon piRNA loss may be due to the progressive accumulation of RNA errors arising from
438 the loss of piRNA-control over splicing rates, and increased misfolded proteins due to an
439 overwhelmed NMD system. Taken together with the known roles of piRNAs in transposon and
440 pseudogene regulation of germline mRNAs, and the growing evidence for links between splicing,

441 genome stability, and transposon activation(*88*), our findings suggest that piRNAs pathway may

442 serve as a conserved node to integrate genome surveillance with RNA and protein quality control.

443 **Acknowledgements**

444 We thank Ms. Selvarasu for microinjection and RT-qPCR experiments, the V.P lab members, and
445 Drs. Eugene Kandel, Katherina Gurova, Andrei Gudkov, Josep Comeron, Anna Malkova and Ana
446 Llopart for comments, Rochester Genomics Research Center for small RNA sequencing and
447 advice, Drs. Paul Quinn and Prashant Singh for mRNA-sequencing, UMI libraries, and advice,
448 and the Caenorhabditis Genetics Center (CGC) (funded by the NIH Infrastructure Programs P40
449 OD010440) for *C. elegans* strains. This work was supported by NIH R01 MH126282 (V.P.), and
450 support for the sequencing core from the National Cancer Institute (NCI) grant P30CA016056 to
451 the Roswell Park Comprehensive Cancer Center.

452 References

453

454 1. E. Z. Shen *et al.*, Identification of piRNA Binding Sites Reveals the Argonaute Regulatory
455 Landscape of the C. elegans Germline. *Cell* **172**, 937-951 e918 (2018).
456 2. H. C. Lee *et al.*, C. elegans piRNAs mediate the genome-wide surveillance of germline
457 transcripts. *Cell* **150**, 78-87 (2012).
458 3. I. Gainetdinov *et al.*, Relaxed targeting rules help PIWI proteins silence transposons.
459 *Nature* **619**, 394-402 (2023).
460 4. P. H. Wu, P. D. Zamore, Defining the functions of PIWI-interacting RNAs. *Nat Rev Mol*
461 *Cell Biol* **22**, 239-240 (2021).
462 5. B. Czech *et al.*, piRNA-Guided Genome Defense: From Biogenesis to Silencing. *Annu*
463 *Rev Genet* **52**, 131-157 (2018).
464 6. D. M. Ozata, I. Gainetdinov, A. Zoch, D. O'Carroll, P. D. Zamore, PIWI-interacting RNAs:
465 small RNAs with big functions. *Nat Rev Genet* **20**, 89-108 (2019).
466 7. A. Ramat, M. Simonelig, Functions of PIWI Proteins in Gene Regulation: New Arrows
467 Added to the piRNA Quiver. *Trends Genet* **37**, 188-200 (2021).
468 8. A. C. Billi, S. E. Fischer, J. K. Kim, Endogenous RNAi pathways in C. elegans.
469 *WormBook*, 1-49 (2014).
470 9. P. Rojas-Rios, M. Simonelig, piRNAs and PIWI proteins: regulators of gene expression
471 in development and stem cells. *Development* **145**, (2018).
472 10. K. Jouravleva, P. D. Zamore, A guide to the biogenesis and functions of endogenous
473 small non-coding RNAs in animals. *Nat Rev Mol Cell Biol* **26**, 347-370 (2025).
474 11. B. F. de Albuquerque, M. Placentino, R. F. Ketting, Maternal piRNAs Are Essential for
475 Germline Development following De Novo Establishment of Endo-siRNAs in
476 Caenorhabditis elegans. *Dev Cell* **34**, 448-456 (2015).

477 12. N. B. Ramakrishna, E. A. Miska, Who watches the watchmen? RNAi pathway-derived
478 ribosomal small RNAs burgeon in absence of piRNAs. *Dev Cell* **56**, 2269-2270 (2021).
479 13. J. Ortega *et al.*, Pachytene piRNAs control discrete meiotic events during
480 spermatogenesis and restrict gene expression in space and time. *Sci Adv* **10**, eadp0466
481 (2024).
482 14. P. Quarato *et al.*, Germline inherited small RNAs facilitate the clearance of untranslated
483 maternal mRNAs in C. elegans embryos. *Nat Commun* **12**, 1441 (2021).
484 15. P. Konstantinidou *et al.*, A comparative roadmap of PIWI-interacting RNAs across seven
485 species reveals insights into de novo piRNA-precursor formation in mammals. *Cell Rep*
486 **43**, 114777 (2024).
487 16. P. J. Batista *et al.*, PRG-1 and 21U-RNAs interact to form the piRNA complex required
488 for fertility in C. elegans. *Mol Cell* **31**, 67-78 (2008).
489 17. D. Zhang *et al.*, The piRNA targeting rules and the resistance to piRNA silencing in
490 endogenous genes. *Science* **359**, 587-592 (2018).
491 18. M. P. Bagijn *et al.*, Function, targets, and evolution of Caenorhabditis elegans piRNAs.
492 *Science* **337**, 574-578 (2012).
493 19. P. P. Das *et al.*, Piwi and piRNAs act upstream of an endogenous siRNA pathway to
494 suppress Tc3 transposon mobility in the Caenorhabditis elegans germline. *Mol Cell* **31**,
495 79-90 (2008).
496 20. W. Gu *et al.*, Distinct argonaute-mediated 22G-RNA pathways direct genome
497 surveillance in the C. elegans germline. *Mol Cell* **36**, 231-244 (2009).
498 21. S. Tu *et al.*, Comparative functional characterization of the CSR-1 22G-RNA pathway in
499 Caenorhabditis nematodes. *Nucleic Acids Res* **43**, 208-224 (2015).
500 22. M. Singh *et al.*, Translation and codon usage regulate Argonaute slicer activity to trigger
501 small RNA biogenesis. *Nat Commun* **12**, 3492 (2021).

502 23. A. Vihervaara, F. M. Duarte, J. T. Lis, Molecular mechanisms driving transcriptional
503 stress responses. *Nat Rev Genet* **19**, 385-397 (2018).
504 24. R. Gomez-Pastor, E. T. Burchfiel, D. J. Thiele, Regulation of heat shock transcription
505 factors and their roles in physiology and disease. *Nat Rev Mol Cell Biol* **19**, 4-19 (2018).
506 25. S. Lindquist, The heat-shock response. *Annu Rev Biochem* **55**, 1151-1191 (1986).
507 26. B. T. Lau, H. P. Ji, Single molecule counting and assessment of random molecular
508 tagging errors with transposable giga-scale error-correcting barcodes. *BMC Genomics*
509 **18**, 745 (2017).
510 27. M. Tsagiopoulou *et al.*, UMIc: A Preprocessing Method for UMI Deduplication and Reads
511 Correction. *Front Genet* **12**, 660366 (2021).
512 28. T. Smith, A. Heger, I. Sudbery, UMI-tools: modeling sequencing errors in Unique
513 Molecular Identifiers to improve quantification accuracy. *Genome Res* **27**, 491-499
514 (2017).
515 29. K. Lebrigand, V. Magnone, P. Barbry, R. Waldmann, High throughput error corrected
516 Nanopore single cell transcriptome sequencing. *Nat Commun* **11**, 4025 (2020).
517 30. K. S. Reid-Bayliss, L. A. Loeb, Accurate RNA consensus sequencing for high-fidelity
518 detection of transcriptional mutagenesis-induced epimutations. *Proc Natl Acad Sci U S A*
519 **114**, 9415-9420 (2017).
520 31. S. Das, S. Min, V. Prahlad, Gene bookmarking by the heat shock transcription factor
521 programs the insulin-like signaling pathway. *Mol Cell* **81**, 4843-4860 e4848 (2021).
522 32. E. M. Weick *et al.*, PRDE-1 is a nuclear factor essential for the biogenesis of Ruby motif-
523 dependent piRNAs in C. elegans. *Genes Dev* **28**, 783-796 (2014).
524 33. C. Weng *et al.*, The USTC co-opts an ancient machinery to drive piRNA transcription in
525 C. elegans. *Genes Dev* **33**, 90-102 (2019).
526 34. C. M. Phillips, D. L. Updike, Germ granules and gene regulation in the Caenorhabditis
527 elegans germline. *Genetics* **220**, (2022).

528 35. M. Ghildiyal, P. D. Zamore, Small silencing RNAs: an expanding universe. *Nat Rev*
529 *Genet* **10**, 94-108 (2009).
530 36. Y. M. Hajdu-Cronin, W. J. Chen, P. W. Sternberg, The L-type cyclin CYL-1 and the heat-
531 shock-factor HSF-1 are required for heat-shock-induced protein expression in
532 Caenorhabditis elegans. *Genetics* **168**, 1937-1949 (2004).
533 37. A. J. Tate, K. C. Brown, T. A. Montgomery, tiny-count: a counting tool for hierarchical
534 classification and quantification of small RNA-seq reads with single-nucleotide precision.
535 *Bioinform Adv* **3**, vbad065 (2023).
536 38. S. Das *et al.*, Serotonin signaling by maternal neurons upon stress ensures progeny
537 survival. *Elife* **9**, (2020).
538 39. C. Y. Jao, A. Salic, Exploring RNA transcription and turnover in vivo by using click
539 chemistry. *Proc Natl Acad Sci U S A* **105**, 15779-15784 (2008).
540 40. M. Rabani *et al.*, Metabolic labeling of RNA uncovers principles of RNA production and
541 degradation dynamics in mammalian cells. *Nat Biotechnol* **29**, 436-442 (2011).
542 41. R. Shalgi, J. A. Hurt, S. Lindquist, C. B. Burge, Widespread inhibition of
543 posttranscriptional splicing shapes the cellular transcriptome following heat shock. *Cell*
544 *Rep* **7**, 1362-1370 (2014).
545 42. J. L. Trincado *et al.*, SUPPA2: fast, accurate, and uncertainty-aware differential splicing
546 analysis across multiple conditions. *Genome Biol* **19**, 40 (2018).
547 43. G. P. Alamancos, A. Pages, J. L. Trincado, N. Bellora, E. Eyras, Leveraging transcript
548 quantification for fast computation of alternative splicing profiles. *RNA* **21**, 1521-1531
549 (2015).
550 44. C. J. Wright, C. W. J. Smith, C. D. Jiggins, Alternative splicing as a source of phenotypic
551 diversity. *Nat Rev Genet* **23**, 697-710 (2022).
552 45. A. Weinreb *et al.*, Alternative splicing across the C. elegans nervous system. *Nat*
553 *Commun* **16**, 4508 (2025).

554 46. N. Frolows, A. Ashe, Small RNAs and chromatin in the multigenerational epigenetic
555 landscape of Caenorhabditis elegans. *Philos Trans R Soc Lond B Biol Sci* **376**,
556 20200112 (2021).
557 47. K. Choquet, I. L. Patop, L. S. Churchman, The regulation and function of post-
558 transcriptional RNA splicing. *Nat Rev Genet* **26**, 378-394 (2025).
559 48. H. E. Merens, K. Choquet, A. R. Baxter-Koenigs, L. S. Churchman, Timing is everything:
560 advances in quantifying splicing kinetics. *Trends Cell Biol* **34**, 968-981 (2024).
561 49. R. Ietswaart *et al.*, Genome-wide quantification of RNA flow across subcellular
562 compartments reveals determinants of the mammalian transcript life cycle. *Mol Cell* **84**,
563 2765-2784 e2716 (2024).
564 50. M. G. Berg *et al.*, U1 snRNP determines mRNA length and regulates isoform expression.
565 *Cell* **150**, 53-64 (2012).
566 51. C. C. Venters, J. M. Oh, C. Di, B. R. So, G. Dreyfuss, U1 snRNP Telescripting:
567 Suppression of Premature Transcription Termination in Introns as a New Layer of Gene
568 Regulation. *Cold Spring Harb Perspect Biol* **11**, (2019).
569 52. J. M. Oh *et al.*, U1 snRNP telescripting regulates a size-function-stratified human
570 genome. *Nat Struct Mol Biol* **24**, 993-999 (2017).
571 53. S. Cugusi *et al.*, Heat shock induces premature transcript termination and reconfigures
572 the human transcriptome. *Mol Cell* **82**, 1573-1588 e1510 (2022).
573 54. A. Y. T. Peng, B. C. Freeman, Inhibiting U1 telescripting: A means to an end for
574 transcription. *Mol Cell* **82**, 1405-1407 (2022).
575 55. M. J. Thomas, A. A. Platas, D. K. Hawley, Transcriptional fidelity and proofreading by
576 RNA polymerase II. *Cell* **93**, 627-637 (1998).
577 56. J. Hwang, L. E. Maquat, Nonsense-mediated mRNA decay (NMD) in animal
578 embryogenesis: to die or not to die, that is the question. *Curr Opin Genet Dev* **21**, 422-
579 430 (2011).

580 57. T. Kurosaki, M. W. Popp, L. E. Maquat, Quality and quantity control of gene expression
581 by nonsense-mediated mRNA decay. *Nat Rev Mol Cell Biol* **20**, 406-420 (2019).
582 58. L. E. Maquat, Nonsense-mediated mRNA decay: splicing, translation and mRNP
583 dynamics. *Nat Rev Mol Cell Biol* **5**, 89-99 (2004).
584 59. L. Johns, A. Grimson, S. L. Kuchma, C. L. Newman, P. Anderson, Caenorhabditis
585 elegans SMG-2 selectively marks mRNAs containing premature translation termination
586 codons. *Mol Cell Biol* **27**, 5630-5638 (2007).
587 60. Q. M. Mitrovich, P. Anderson, mRNA surveillance of expressed pseudogenes in C.
588 elegans. *Curr Biol* **15**, 963-967 (2005).
589 61. V. S. Muir, A. P. Gasch, P. Anderson, The Substrates of Nonsense-Mediated mRNA
590 Decay in Caenorhabditis elegans. *G3 (Bethesda)* **8**, 195-205 (2018).
591 62. R. Pulak, P. Anderson, mRNA surveillance by the Caenorhabditis elegans smg genes.
592 *Genes Dev* **7**, 1885-1897 (1993).
593 63. J. Hodgkin, A. Papp, R. Pulak, V. Ambros, P. Anderson, A new kind of informational
594 suppression in the nematode Caenorhabditis elegans. *Genetics* **123**, 301-313 (1989).
595 64. F. K. Teixeira *et al.*, piRNA-mediated regulation of transposon alternative splicing in the
596 soma and germ line. *Nature* **552**, 268-272 (2017).
597 65. J. He *et al.*, piRNA-guided intron removal from pre-mRNAs regulates density-dependent
598 reproductive strategy. *Cell Rep* **39**, 110593 (2022).
599 66. A. Akay *et al.*, The Helicase Aquarius/EMB-4 Is Required to Overcome Intronic Barriers
600 to Allow Nuclear RNAi Pathways to Heritably Silence Transcription. *Dev Cell* **42**, 241-255
601 e246 (2017).
602 67. K. M. Tyc *et al.*, The Conserved Intron Binding Protein EMB-4 Plays Differential Roles in
603 Germline Small RNA Pathways of C. elegans. *Dev Cell* **42**, 256-270 e256 (2017).
604 68. Y. V. Makeyeva, M. Shirayama, C. C. Mello, Cues from mRNA splicing prevent default
605 Argonaute silencing in C. elegans. *Dev Cell* **56**, 2636-2648 e2634 (2021).

606 69. S. Medvedeva *et al.*, Widespread and intron-rich mirusviruses are predicted to
607 reproduce in nuclei of unicellular eukaryotes. *Nat Microbiol*, (2025).
608 70. A. V. Sverdlov, I. B. Rogozin, V. N. Babenko, E. V. Koonin, Evidence of splice signal
609 migration from exon to intron during intron evolution. *Curr Biol* **13**, 2170-2174 (2003).
610 71. R. J. Ross, M. M. Weiner, H. Lin, PIWI proteins and PIWI-interacting RNAs in the soma.
611 *Nature* **505**, 353-359 (2014).
612 72. D. E. Golden, V. R. Gerbasi, E. J. Sontheimer, An inside job for siRNAs. *Mol Cell* **31**,
613 309-312 (2008).
614 73. J. S. Khanduja, I. A. Calvo, R. I. Joh, I. T. Hill, M. Motamedi, Nuclear Noncoding RNAs
615 and Genome Stability. *Mol Cell* **63**, 7-20 (2016).
616 74. L. Peters, G. Meister, Argonaute proteins: mediators of RNA silencing. *Mol Cell* **26**, 611-
617 623 (2007).
618 75. A. G. Seto, R. E. Kingston, N. C. Lau, The coming of age for Piwi proteins. *Mol Cell* **26**,
619 603-609 (2007).
620 76. T. Watanabe, H. Lin, Posttranscriptional regulation of gene expression by Piwi proteins
621 and piRNAs. *Mol Cell* **56**, 18-27 (2014).
622 77. S. Pritam, S. Signor, Evolution of piRNA-guided defense against transposable elements.
623 *Trends Genet* **41**, 390-401 (2025).
624 78. M. Abajorga, L. Yurkovetskiy, J. Luban, piRNA Defense Against Endogenous
625 Retroviruses. *Viruses* **16**, (2024).
626 79. P. Sarkies *et al.*, Ancient and novel small RNA pathways compensate for the loss of
627 piRNAs in multiple independent nematode lineages. *PLoS Biol* **13**, e1002061 (2015).
628 80. J. P. T. Ouyang, G. Seydoux, Nuage condensates: accelerators or circuit breakers for
629 sRNA silencing pathways? *RNA* **28**, 58-66 (2022).
630 81. F. A. Kondrashov, E. V. Koonin, Origin of alternative splicing by tandem exon duplication.
631 *Hum Mol Genet* **10**, 2661-2669 (2001).

632 82. F. A. Kondrashov, E. V. Koonin, Evolution of alternative splicing: deletions, insertions and
633 origin of functional parts of proteins from intron sequences. *Trends Genet* **19**, 115-119
634 (2003).
635 83. A. M. Resch, A. Y. Ogurtsov, I. B. Rogozin, S. A. Shabalina, E. V. Koonin, Evolution of
636 alternative and constitutive regions of mammalian 5'UTRs. *BMC Genomics* **10**, 162
637 (2009).
638 84. H. Keren, G. Lev-Maor, G. Ast, Alternative splicing and evolution: diversification, exon
639 definition and function. *Nat Rev Genet* **11**, 345-355 (2010).
640 85. M. Simon *et al.*, Reduced insulin/IGF-1 signaling restores germ cell immortality to
641 Caenorhabditis elegans Piwi mutants. *Cell Rep* **7**, 762-773 (2014).
642 86. H. G. Son *et al.*, RNA surveillance via nonsense-mediated mRNA decay is crucial for
643 longevity in daf-2/insulin/IGF-1 mutant C. elegans. *Nat Commun* **8**, 14749 (2017).
644 87. E. J. E. Kim *et al.*, Caenorhabditis elegans algn-2 Is Critical for Longevity Conferred by
645 Enhanced Nonsense-Mediated mRNA Decay. *iScience* **23**, 101713 (2020).
646 88. P. A. Dumesic, H. D. Madhani, The spliceosome as a transposon sensor. *RNA Biol* **10**,
647 1653-1660 (2013).
648

Figure 1

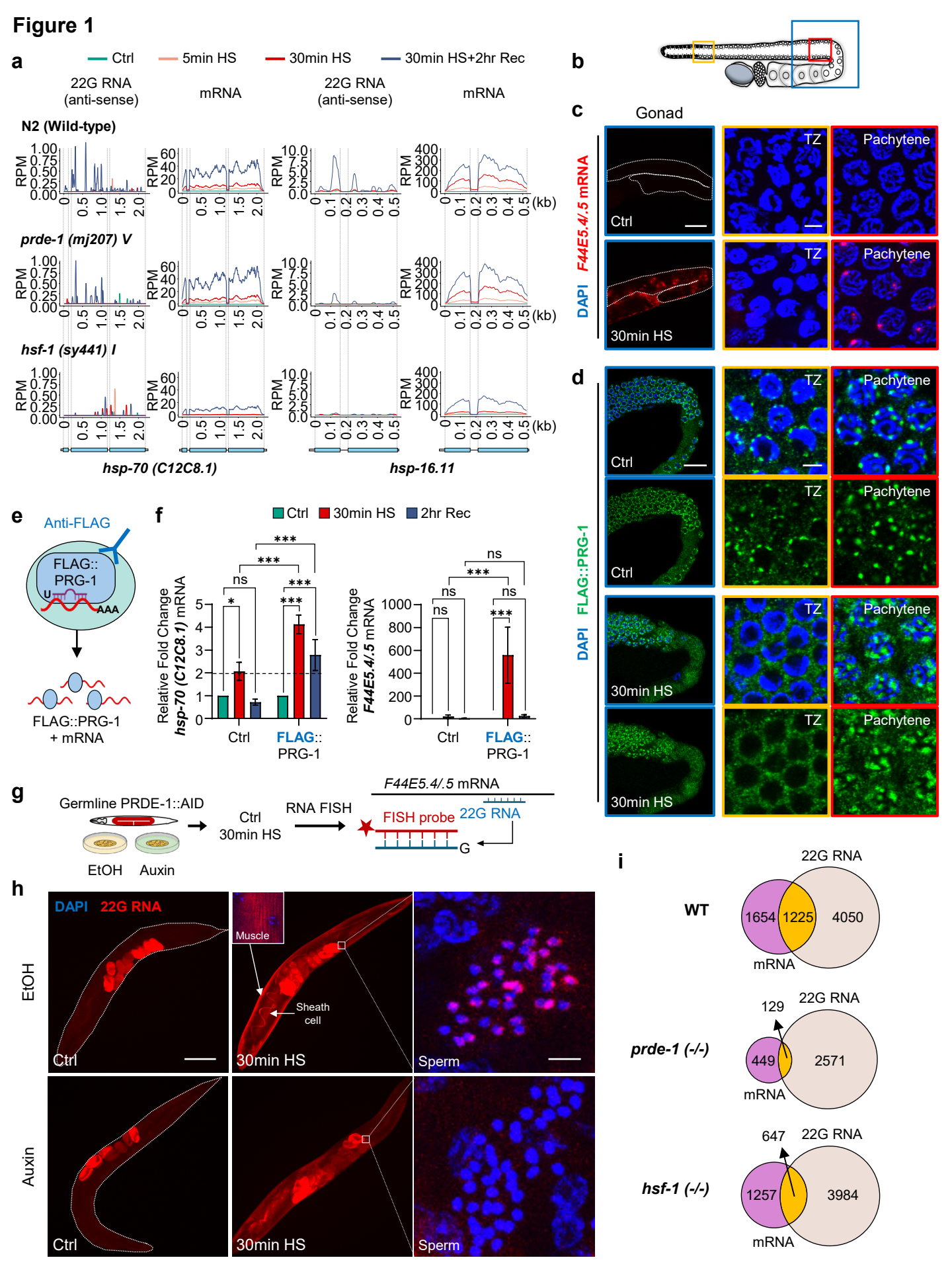
a
Ctrl
5min HS
30min HS
30min HS+2hr Rec
22G RNA (anti-sense)
mRNA
22G RNA (anti-sense)
mRNA
N2 (Wild-type)
prde-1 (mj207) V
hsf-1 (sy441) I
RPM
(kb)
hsp-70 (C12C8.1)
hsp-16.11
b
c
Gonad
F44E5.4/.5 mRNA
DAPI
Ctrl
30min HS
TZ
Pachytene
d
FLAG::PRG-1
DAPI
Ctrl
30min HS
TZ
Pachytene
e
Anti-FLAG
FLAG:: PRG-1
U
AAA
FLAG::PRG-1 + mRNA
f
Ctrl
30min HS
2hr Rec
Relative Fold Change hsp-70 (C12C8.1) mRNA
Relative Fold Change F44E5.4/.5 mRNA
ns
*
***
Ctrl
FLAG:: PRG-1
g
Germline PRDE-1::AID
EtOH
Auxin
Ctrl
30min HS
RNA FISH
F44E5.4/.5 mRNA
FISH probe
22G RNA
G
h
DAPI
22G RNA
EtOH
Auxin
Muscle
Sheath cell
Ctrl
30min HS
Sperm
i
WT
22G RNA
mRNA
1654
1225
4050
prde-1 (-/-)
129
449
2571
hsf-1 (-/-)
647
1257
3984

Figure 1. Piwi-interacting RNAs (piRNAs) target *hsp* mRNAs upon heat shock.

a. Metaprofile plots showing normalized antisense 22G-RNA reads (RPM), and mRNA reads (RPM) across *hsp* mRNAs in wild-type (WT, *C. elegans* wild isolate, var Bristol), *prde-1(mj207) V,* and *hsf-1(sy441) I* mutants. **Top**: conditions of heat shock. **Bottom**: Schematic of *hsp* genes analyzed.

b-d. Spatial localization of *hsp-70* mRNA and PIWI (PRG-1) in the WT germlines. **(b)** Schematic of gonad regions in **c** and **d**: Blue box, Gonad region shown. Orange box, transition zone (TZ). Red box, Late pachytene. Representative confocal images of each region showing **(c)** *hsp-70 (F44E5.4/.5)* mRNA localized using RNA Fluorescence *in situ* hybridization (RNA FISH; Projected image), and **(d)** PIWI (FLAG::PRG-1) by immunostaining with anti-FLAG antibody (Z-section). Germlines from non-heat-shocked (Ctrl) and heat-shock-exposed (30min HS) animals are shown. Red: *hsp-70 (F44E5.4/.5)* mRNA. Green: FLAG::PRG-1. Blue: DNA staining with DAPI. Scale bars, c: 50 μm (Gonad), and 3 μm (TZ, Pachytene). Scale bars, d: 20 μm (Gonad), and 3 μm (TZ, Pachytene).

e, f. Native RNA immunoprecipitation (RIP) to probe *hsp* mRNA's association with PIWI (FLAG::PRG-1). **(e)** Experiment Schematic. **(f)** Relative fold change (RT-qPCR) in *hsp-70s* (*C12C8.1* and *F44E5.4/.5*) mRNAs that immunoprecipitated with PIWI. *hsp* mRNA levels were normalized to *pmp*-3 (input) and are shown relative to non-heat-shocked animals. Ctrl: wild-type animals with no FLAG-tagged proteins were negative controls. *bath-45* served as positive control (Suppl. Fig 2b). Legend: Treatment conditions. Bars: mean value. Error bars: standard error. n = 3-5 biologically independent experiments. Statistical analysis: 2-way ANOVA.

g, h. Germline depletion of PRDE-1 using the auxin-inducible degron (AID) system followed by RNA FISH to detect 22G-RNAs antisense to *hsp-70 (F44E5.4/.5).* **(g)** Experiment schematic: EtOH: Vehicle control. Probe design shown. **(h)** Representative micrographs (projected confocal Z-sections) showing RNA FISH of 22G-RNA under control conditions (EtOH) and upon PRDE-1 depletion (auxin). Red: 22G-RNA. Blue: DAPI stained DNA. Expression in muscle (arrow, box) and gonad sheath cells (arrow), and in sperm (highlighted). Embryos staining is non-specific. Scale bars: 100 μm (Ctrl, 30min HS), and 3 μm (Sperm).

i. Venn diagrams showing overlap between differentially expressed mRNAs and 22G-RNAs upon 30 minutes heat shock in WT, *prde-1* and *hsf-1* mutants.

Figure 2

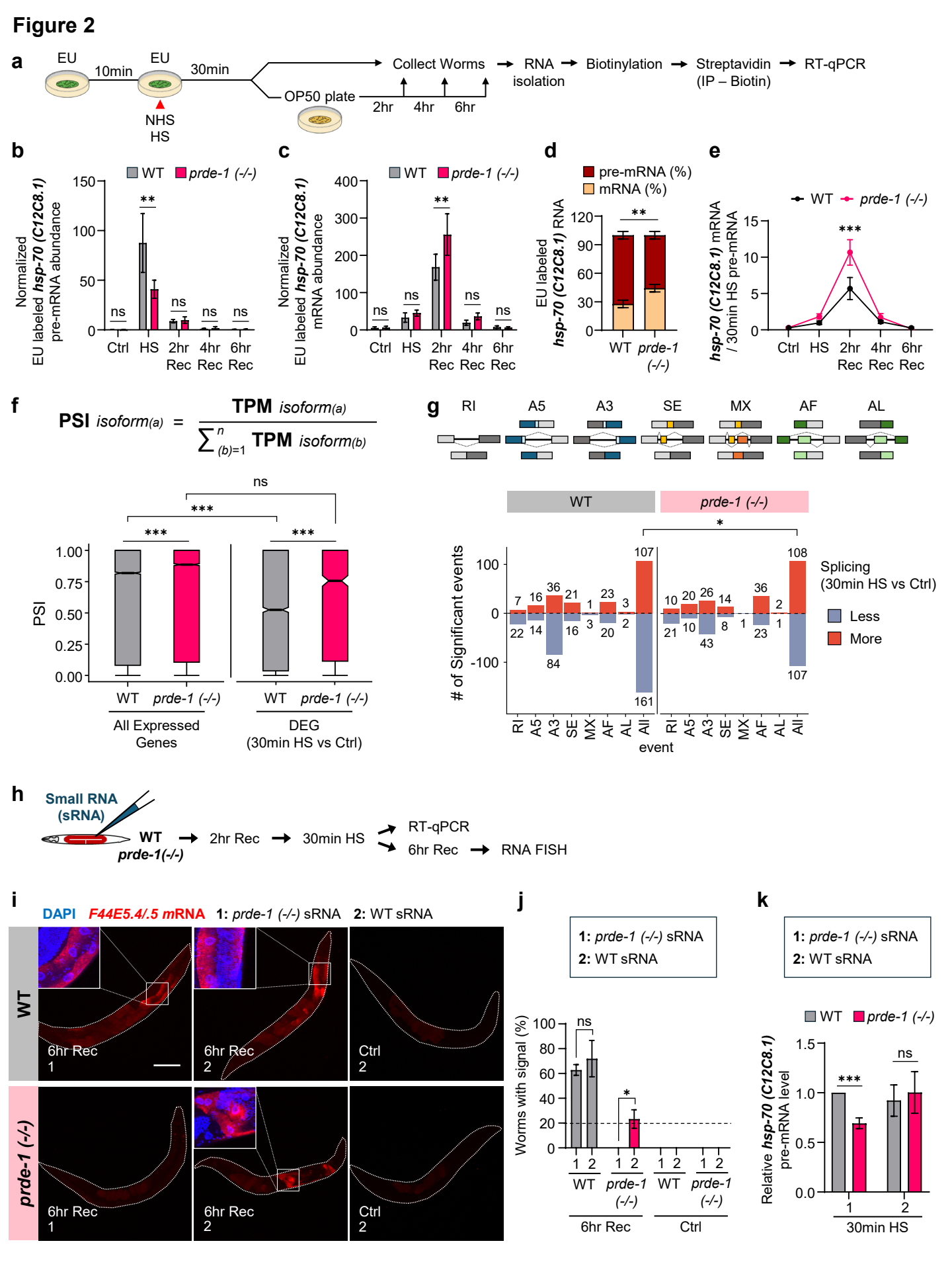
a
EU
10min
EU
30min
NHS
HS
OP50 plate
2hr
4hr
6hr
Collect Worms
RNA isolation
Biotinylation
Streptavidin (IP – Biotin)
RT-qPCR
b
WT
prde-1 (-/-)
Normalized EU labeled hsp-70 (C12C8.1) pre-mRNA abundance
Ctrl
HS
2hr Rec
4hr Rec
6hr Rec
c
Normalized EU labeled hsp-70 (C12C8.1) mRNA abundance
d
pre-mRNA (%)
mRNA (%)
EU labeled hsp-70 (C12C8.1) RNA
e
hsp-70 (C12C8.1) mRNA / 30min HS pre-mRNA
f
PSI isoform(a) = TPM isoform(a) / Σ(b)=1 n TPM isoform(b)
PSI
All Expressed Genes
DEG (30min HS vs Ctrl)
g
RI
A5
A3
SE
MX
AF
AL
# of Significant events
Splicing (30min HS vs Ctrl)
Less
More
event
All
h
Small RNA (sRNA)
WT
prde-1(-/-)
2hr Rec
30min HS
RT-qPCR
6hr Rec
RNA FISH
i
DAPI
F44E5.4/.5 mRNA
1: prde-1 (-/-) sRNA
2: WT sRNA
6hr Rec 1
6hr Rec 2
Ctrl 2
j
Worms with signal (%)
6hr Rec
Ctrl
k
Relative hsp-70 (C12C8.1) pre-mRNA level
30min HS

Figure 2. piRNAs delay *hsp* mRNAs splicing.

a-e. Metabolic pulse-chase labeling with EU and quantification of *hsp* RNA. **(a)** Experiment schematic: animals were fed EU-mixed bacteria 10 minutes before heat shock (pre-loading), heat shocked for 30 minutes (pulse-labeling nascent RNA), and moved onto unlabeled bacterial plates (chase). The EU-labeled nascent RNA was isolated from NHS animals (Ctrl), heat-shocked animals immediately after 30 min heat-shock (HS), and after 2,4, and 6 hrs post-heat shock recovery (Rec), biotin-conjugated, and immunoprecipitated. Normalized absolute RNA abundance was quantified by RT-qPCR (see methods; *pmp-3* mRNA used to normalize for variability in labeling). EU-labeled *hsp-70 (C12C8.1)* **(b)** pre-mRNA and **(c)** mRNA abundance. Y-axis: Normalized abundance. X-axis: Treatments. Note EU-labeled mRNA is derived from the splicing of EU-labeled pre-mRNA. **(d)** Percentages of pre-mRNA and mRNA in total EU-labeled RNA after 30 min heat shock. **(e)** Relative amounts of EU-labeled spliced mRNAs produced from the nascent EU-labeled unspliced pre-mRNA. Values normalized to *pmp-3*. Y-axis: Relative abundance. X-axis: Treatment. Bars (b-d) and line graph (e): mean value. Error bars: standard error. (b, c, e) n = 5-13 biologically independent experiments. Statistical analysis: 2 way-ANOVA; (d) n = 14 biologically independent experiments. Statistical analysis: two-tailed unpaired t-test.

f. Genes differentially regulated by heat shock in WT, but not *prde-1* animals, are enriched for alternative spliced isoforms. **Top**: Calculation of PSI “percent spliced in” values. **Bottom**: Alternative spliced isoforms, as reflected by PSI values, in all expressed genes, and in differentially expressed genes (p.adj <0.05) in wild-type and *prde-1* animals. Boxplots: median value depicted. Error bars: standard error. Statistical analysis: two-tailed unpaired t-test.

g. Alternative splicing (AS) events in WT and *prde-1* animals upon heat shock. **Top**: AS events, retained intron (RI), alternative 5'/3' Splice Sites (A5/A3), skipped exon (SE), mutually exclusive

exons (MX), and alternative first and last exons (AF/AL). **Bottom**: Number of AS events amongst differentially expressed genes (HS vs NHS condition; p.adj <0.05) in WT and *prde-1* mutants. Bars: Number of events (splicing increase or decrease relative to NHS condition). Statistical analysis: Chi-square analysis.

h-j. Microinjection of small RNA fractions isolated from WT animals rescues *hsp*-70 fate. **(h)** Experiment schematic: small RNA fractions purified from heat-shocked WT and *prde-1* animals were injected into WT and *prde-1* animals shortly before heat-shock exposure, and animals were probed for *hsp-70 (F44E5.4/.5)* 6 hours post-heat shock. Non-heat-shocked animals were injected to control for effects of injection alone. **(i)** RNA FISH of *hsp-70 (F44E5.4/.5)* in WT and *prde-1* animals 6 hours following heat shock or under NHS conditions. Injection mix (box) and treatment indicated. Red: *hsp-70 (F544E5.4/.5)* mRNA. Blue: DNA staining with DAPI. Scale bars: 100 µm. **(j)** Quantification of results. Y-axis: Percentage of injected animals positive for *hsp-70*. X-axis: Injection mix, strains and treatment. Bars: mean value. Error bars: standard error. n = 17-22 worms (6hr Rec), 6-10 worms (Ctrl). Statistical analysis: Fisher's exact test.

k. Microinjection of small RNA fractions isolated from heat-shocked WT animals rescues *hsp*-70 pre-mRNA levels. Normalized RT-qPCR of relative fold change of *hsp-70* (*C12C8.1*) pre-mRNAs following sRNA injection. Y-axis: *hsp-70* pre-mRNA levels, normalized to *pmp-3*, relative to heat-shocked wild-type animals injected with small RNAs from *prde-1* mutants. X-axis: Injection mix (see box in Fig 2g). Bars: mean value. Error bars: standard error. n = 6 biologically independent experiments. Statistical analysis: two-tailed unpaired t-test.

Figure 3

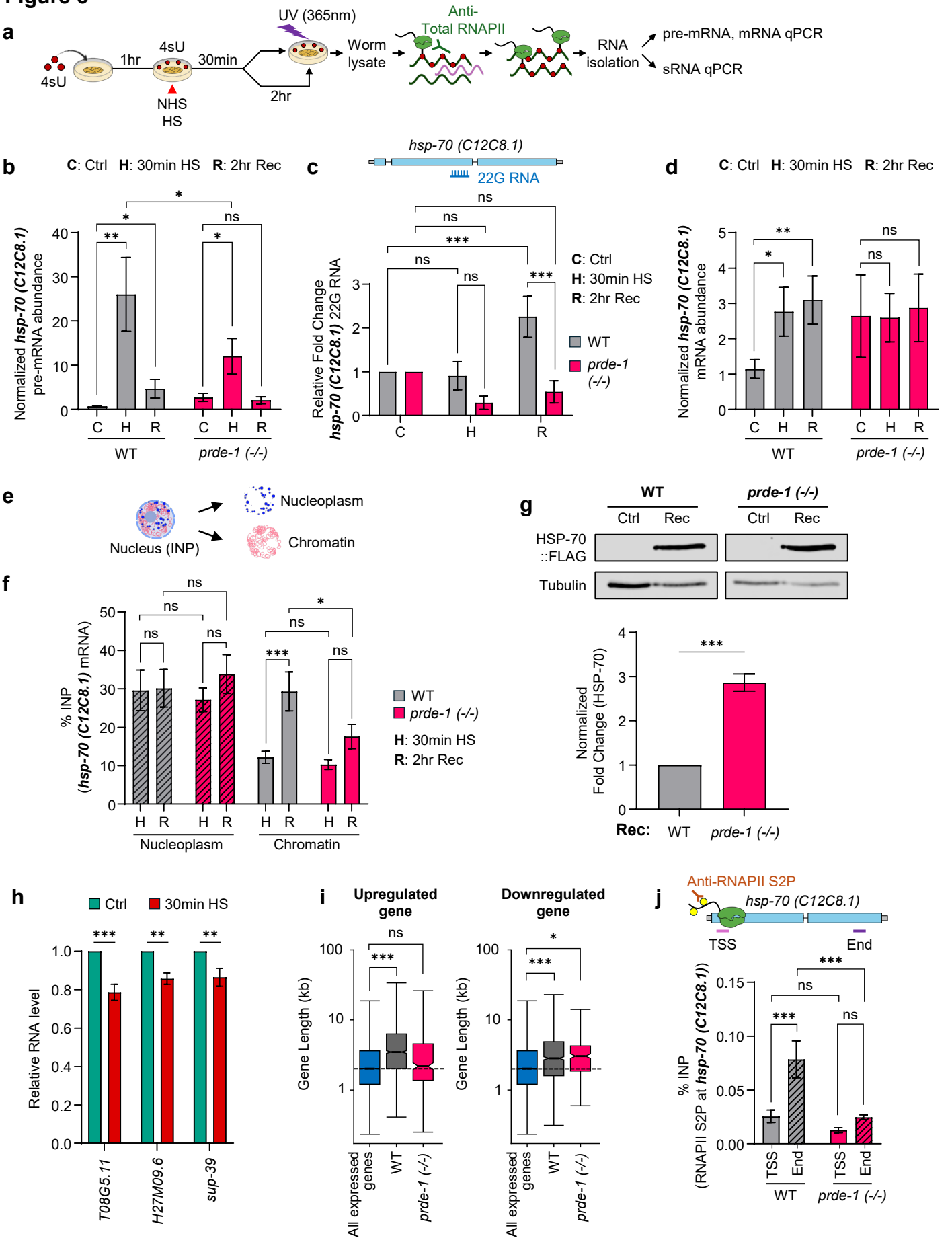
a
4sU
1hr
4sU
NHS
HS
30min
UV (365nm)
2hr
Worm lysate
Anti-Total RNAPII
RNA isolation
pre-mRNA, mRNA qPCR
sRNA qPCR
b
C: Ctrl H: 30min HS R: 2hr Rec
Normalized hsp-70 (C12C8.1) pre-mRNA abundance
WT
prde-1 (-/-)
c
hsp-70 (C12C8.1)
22G RNA
Relative Fold Change hsp-70 (C12C8.1) 22G RNA
C: Ctrl
H: 30min HS
R: 2hr Rec
WT
prde-1 (-/-)
d
C: Ctrl H: 30min HS R: 2hr Rec
Normalized hsp-70 (C12C8.1) mRNA abundance
WT
prde-1 (-/-)
e
Nucleus (INP)
Nucleoplasm
Chromatin
f
% INP (hsp-70 (C12C8.1) mRNA)
WT
prde-1 (-/-)
H: 30min HS
R: 2hr Rec
Nucleoplasm
Chromatin
g
WT
prde-1 (-/-)
Ctrl
Rec
HSP-70 ::FLAG
Tubulin
Normalized Fold Change (HSP-70)
Rec:
WT
prde-1 (-/-)
h
Ctrl
30min HS
Relative RNA level
T08G5.11
H27M09.6
sup-39
i
Upregulated gene
Downregulated gene
Gene Length (kb)
All expressed genes
WT
prde-1 (-/-)
j
Anti-RNAPII S2P
hsp-70 (C12C8.1)
TSS
End
% INP (RNAPII S2P at hsp-70 (C12C8.1))
WT
prde-1 (-/-)

Figure 3. Antisense 22G-RNAs associated with RNA Polymerase II at the transcription complex to modulate post-transcriptional splicing.

a-d. Modified PAR-CLIP to assess 22G-RNAs' role in splicing. **(a)** Experiment schematic: Animals were fed 4sU-mixed bacteria, subjected to heat shock, exposed to UV (365 nm) either immediately or after 2 hours of recovery, RNA Pol II was immunoprecipitated, *hsp* mRNA and pre-mRNA were quantified by computing absolute RNA abundance (RT-qPCR and standard curves; *pmp-3* mRNA used to normalize for variability in IP amounts across samples and experiments) and 22G-RNA quantified as relative fold change using stem loop PCR (design shown). See Suppl. Fig 7c for details. Amounts of **(b)** *hsp-70 (C12C8.1)* pre-mRNA, **(c)** 22G-RNA, and **(d)** *hsp-70 (C12C8.1)* mRNA that cross-linked to, and immunoprecipitated with Pol II. Y-axis: Normalized or relative abundance. X-axis: Treatment conditions (see top legend). Bars: mean value. Error bars: standard error. (b) n = 8-13 biologically independent experiments. Statistical analysis: two-tailed unpaired t-test (within strain) and 2-way ANOVA (between strains); (c) n = 5-6 biologically independent experiments. Statistical analysis: 2-way ANOVA; (d) n = 5-10 biologically independent experiments. Statistical analysis: 2-way ANOVA.

e, f. Nuclear fractionation to assess chromatin retention of *hsp-70* RNA. **(e)** Experiment schematic. Nuclei were isolated, fractionated to obtain nucleoplasm and chromatin, and enrichment of *hsp-70* mRNA in both fractions was determined. **(f)** Fold enrichment over input (nuclei) of *hsp-70 (C12C8.1)* mRNA in respective fractions. Y-axis: % input (total nucleus). X-axis: Nuclear fraction, strain, and treatment. Bars: mean value. Error bars: standard error. n = 9-10 biologically independent experiments. Statistical analysis: 2-way ANOVA.

g. HSP-70 protein levels in WT and *prde-1.* **Top:** Representative western blot image showing HSP-70(C12C8.1)::FLAG in NHS (Ctrl) or after heat-shock in WT and *prde-1* animals expressing

endogenous *flag*-tagged *hsp-70*. Animals harvested 3 hrs following HS (Rec) to allow HSP-70 protein synthesis. Tubulin: loading control. **Bottom:** Relative HSP-70 protein expression (relative to wild-type heat-shocked levels, because control animals do not express detectable HSP-70 protein). Bars: mean value. Error bars: standard error. n = 3 biologically independent experiments. Statistical analysis: two-tailed unpaired t-test.

h. U1 RNA levels upon heat shock in WT animals (RT-qPCR: relative fold change). U1 RNA values normalized to *pmp-3* mRNA values and shown relative to NHS levels. Y-axis: Relative RNA levels. X-axis: U1 RNAs. Bars: mean value. Error bars: standard error. n = 3-4 biologically independent experiments. Statistical analysis: 2-way ANOVA.

i. Gene length dependence of heat-shock upregulated and downregulated protein-coding genes (p.adj <0.05). Y-axis: Average gene lengths (kb). X-axis: Strain. Genome-wide gene lengths of all expressed genes depicted for comparison. Boxplots: median value depicted. Error bars: standard error. Statistical analysis: Tukey HSD.

j. Elongating RNA polymerase II (anti-S2P) levels at *hsp* gene. **Top:** Schematic of *hsp-70 (C12C8.1)* gene, and regions probed: Transcription Start Site (TSS) and distal regions (3') of *hsp-70* (*C12C8.1*). **Bottom:** ChIP-qPCR showing fold enrichment over input. Y-axis: % ChIP input. X-axis: Strain, and region assayed. Bars: mean value. Error bars: standard error. n = 4-8 biologically independent experiments. Statistical analysis: 2-way ANOVA.

Figure 4

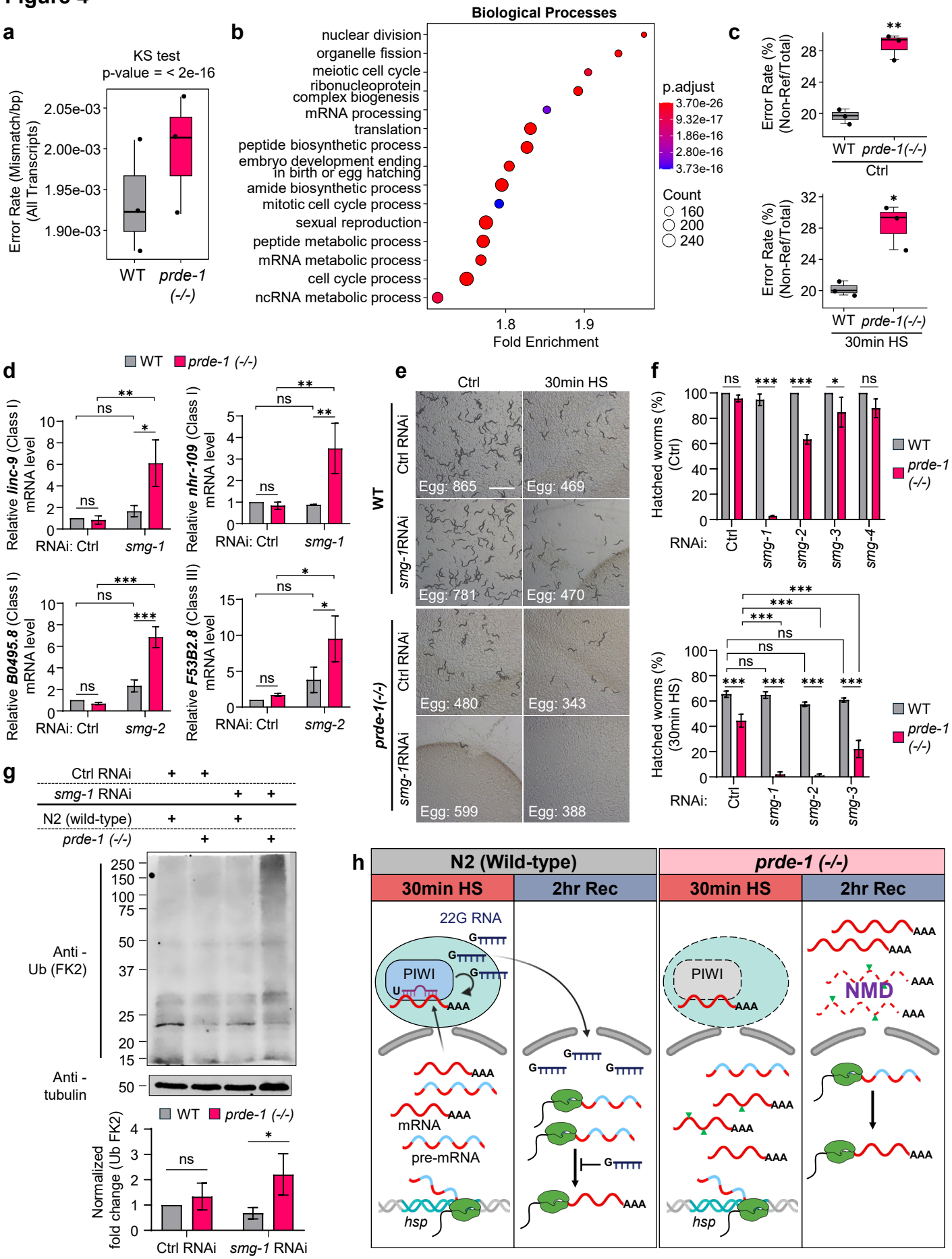
a
KS test
p-value = < 2e-16
Error Rate (Mismatch/bp) (All Transcripts)
2.05e-03
2.00e-03
1.95e-03
1.90e-03
WT
prde-1 (-/-)
b
Biological Processes
nuclear division
organelle fission
meiotic cell cycle
ribonucleoprotein complex biogenesis
mRNA processing
translation
peptide biosynthetic process
embryo development ending in birth or egg hatching
amide biosynthetic process
mitotic cell cycle process
sexual reproduction
peptide metabolic process
mRNA metabolic process
cell cycle process
ncRNA metabolic process
1.8
1.9
Fold Enrichment
p.adjust
3.70e-26
9.32e-17
1.86e-16
2.80e-16
3.73e-16
Count
160
200
240
c
Error Rate (%) (Non-Ref/Total)
WT
prde-1(-/-)
Ctrl
30min HS
d
WT
prde-1 (-/-)
Relative linc-9 (Class I) mRNA level
Relative nhr-109 (Class I) mRNA level
Relative B0495.8 (Class I) mRNA level
Relative F53B2.8 (Class III) mRNA level
RNAi: Ctrl
smg-1
smg-2
ns
e
Ctrl
30min HS
WT
prde-1(-/-)
Ctrl RNAi
smg-1RNAi
Egg: 865
Egg: 469
Egg: 781
Egg: 470
Egg: 480
Egg: 343
Egg: 599
Egg: 388
f
Hatched worms (%) (Ctrl)
Hatched worms (%) (30min HS)
RNAi:
Ctrl
smg-1
smg-2
smg-3
smg-4
WT
prde-1 (-/-)
g
Ctrl RNAi
smg-1 RNAi
N2 (wild-type)
prde-1 (-/-)
Anti - Ub (FK2)
Anti - tubulin
Normalized fold change (Ub FK2)
Ctrl RNAi
smg-1 RNAi
h
N2 (Wild-type)
prde-1 (-/-)
30min HS
2hr Rec
22G RNA
PIWI
AAA
mRNA
pre-mRNA
hsp
NMD

Figure 4. piRNA protects transcript fidelity and complements nonsense-mediated decay (NMD) to maintain protein quality control.

a. Mean error rate per nucleotide for all transcripts (generated from 'pileup') in wild type and *prde-1* mutants. Y-axis: Mean error rate (mismatches per bp). X-axis: strain. Approximately 3.71 x 10^7 individual mRNAs analyzed per biological replicate per strain. See **Methods** for details. Boxplots: median value depicted. Error bars: standard error. Statistical analysis: Kolmogorov-Smirnov (KS) test

b. Gene Ontology analysis for transcripts with higher error rate in *prde-1* animals versus wild type.

c. Variant error rates in differentially expressed genes (p.adj <0.05) between wild type and *prde-1* mutants (variants identified by GATK Haplotype Caller and SnpEff). **Top:** Control conditions. **Bottom:** Heat shock conditions. Y-axis: % variants. X-axis: Strain. Boxplots: median value depicted. Error bars: standard error. Statistical analysis: two-tailed unpaired t-test.

d. Hyperactivation of NMD in *prde-1* animals. NMD-related gene expression levels in WT and *prde-1* animals on Ctrl (L4440) and *smg-1* or *smg-2* RNAi (RT-qPCR: relative fold change). 3 Class I NMD targets (*linc-9*, *nhr-109*, *B0495.8*) and 1 Class III NMD target (*F53B2.8*) expression values normalized to *eft-3* mRNA values and shown relative to wild-type Control RNAi-treated animals. Y-axis: Relative RNA levels. X-axis: RNAi-treatment. Bars: mean value. Error bars: standard error. n = 4-6 biologically independent experiments. Statistical analysis: 2-way ANOVA.

e-f. NMD dependence of *prde-1* animals. **(e)** Representative DIC micrographs of progeny from control and heat-shocked WT and *prde-1* animals on Ctrl (L4440) and *smg-1* RNAi. The number of eggs laid by the mothers in one representative experiment is shown. Note: WT progeny have

grown into adults. Scale bar: 2mm. **(f)** Percent viable embryos from mothers subjected to RNAi-mediated downregulation of NMD components under **(Top)** control, and **(Bottom)** heat shock conditions. Y-axis: Percentage of viable embryos. X-axis: RNAi-treatment. Bars: mean value. Error bars: standard error. n = 3-5 biologically independent experiments. Statistical analysis: 2 way-ANOVA.

g. Polyubiquitinated protein levels in WT and *prde*-1animals exposed to control (L4440) or *smg-1* RNAi. **Top:** Representative western blot (antibody:clone FK2). Tubulin: loading control. **Bottom:** Quantification of polyubiquitinated protein (normalized to wild-type Control RNAi-treated animals). Bars: mean value. Error bars: standard error. n = 5 biologically independent experiments. Statistical analysis: 2 way-ANOVA.

h. Model for the mechanism through which piRNA/22G-RNA pathway enforces RNA quality. In the presence of piRNA, splicing rates are restrained, thereby preserving RNA fidelity. In the absence of piRNAs, splicing is precocious, mRNAs accumulate errors, and NMD is hyperactivated to eliminate erroneous transcripts.

Suppl. Figure 1

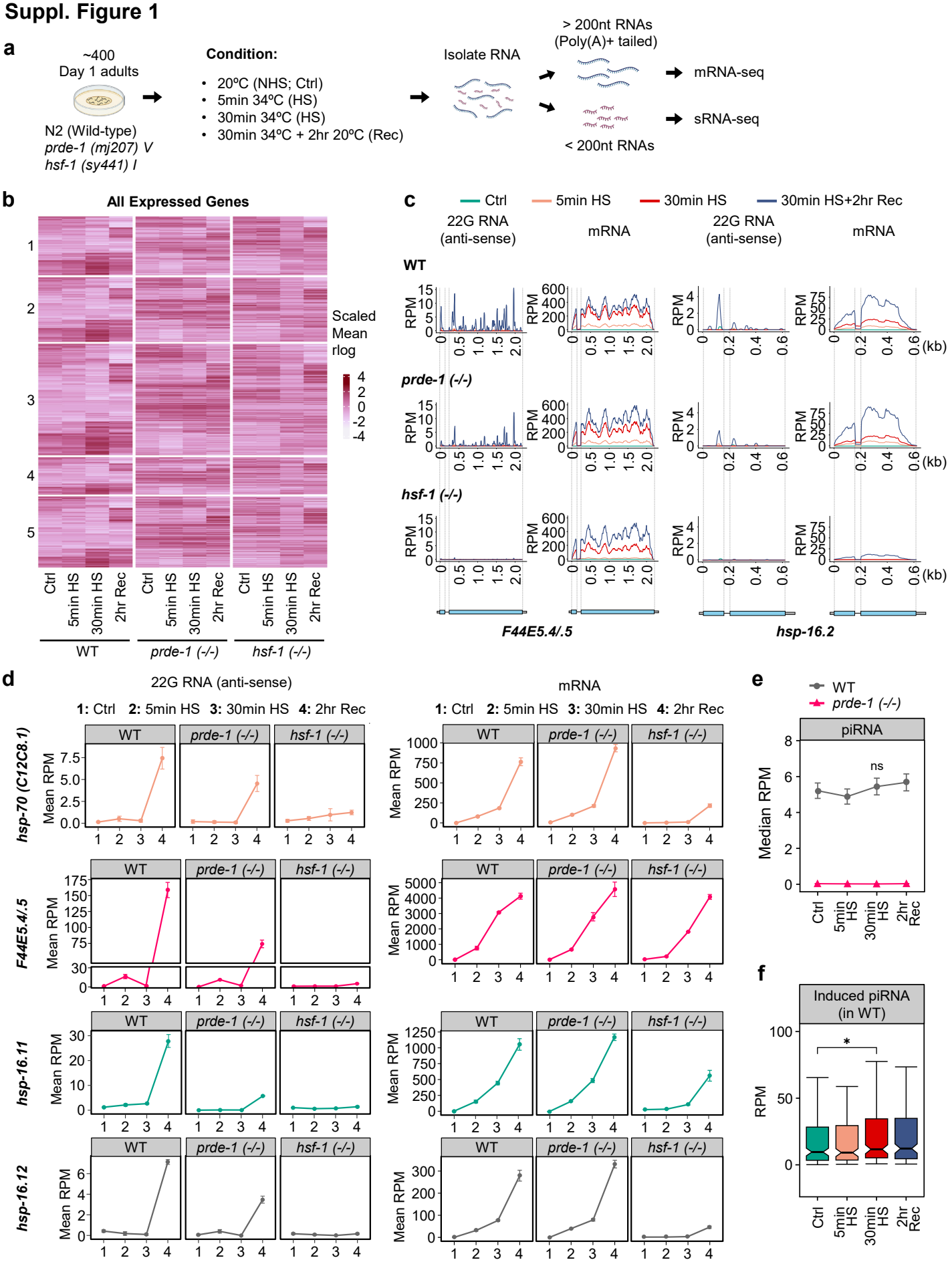

Supplementary Figure 1. Piwi-interacting RNAs (piRNAs) target *hsp* mRNAs upon heat shock.

a. RNA-sequencing experiment schematic.

b. Heatmaps: Wild type (N2; WT, left), *prde-1* (middle), and *hsf-1* (right). Mean expression values of the regularized log (rlog) transformed counts for all expressed genes shown for each strain. Expression scaled row-wise (z-score) to highlight relative changes. K-means clustering was performed on the gene expression of the WT samples, and gene order and clustering (1-5) are preserved across strains and treatments. Columns: treatments [Non heat shocked control (NHS; Ctrl), 5 minutes heat shock (5min HS), 30 minutes heat shock (30min HS), and 2 hours recovery (2hr Rec)]. Color bar: scaled expression level.

c. Metaprofile plots showing normalized antisense 22G-RNA reads (RPM), and mRNA reads (RPM) across *hsp* mRNAs in wild-type (WT), *prde-1* and *hsf-1* mutants. **Top**: Conditions of heat shock. **Bottom**: Schematic of *hsp* genes analyzed.

d. Left: Normalized expression (RPM) of 22G-RNAs antisense to *hsp* genes. **Right:** Normalized expression (PRM) of *hsp* mRNAs in WT, *prde*-1, and *hsf-1* mutants. Y-axis: Expression (RPM). X-axis: Treatments (see top legend).

e. Normalized expression (RPM) of piRNAs in WT and *prde*-1 mutants. RPM >0.5 in at least one sample and RPM >0 in at least replicates were counted. Statistical analysis: Wilcoxon test.

f. Boxplot showing normalized expression (RPM) of significantly differentially expressed piRNAs between the WT 30 minutes heat shock and control conditions. Boxplots: median value depicted. Y-axis: Expression (RPM). X-axis: Treatments. Statistical analysis: Wilcoxon test.

Suppl. Figure 2

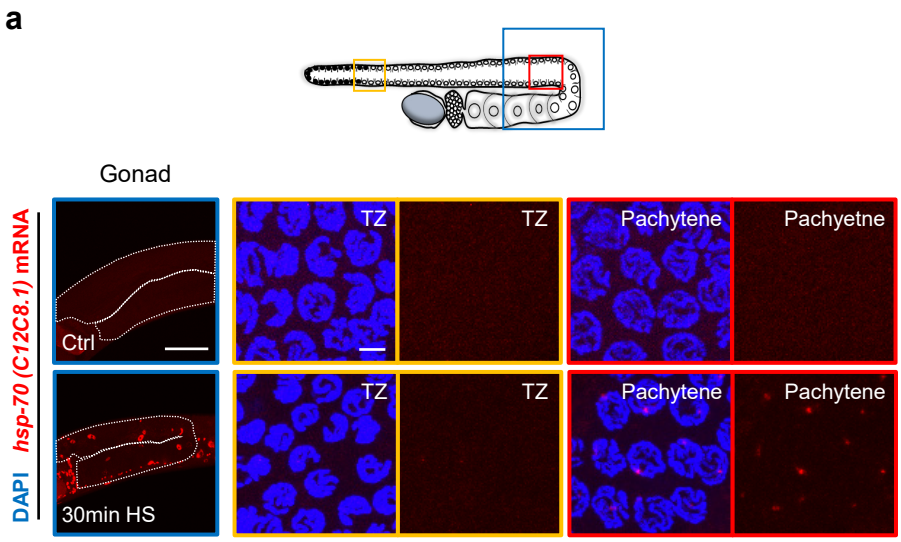

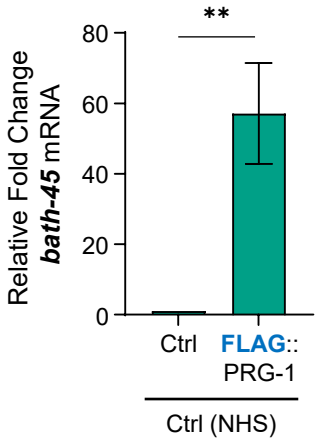

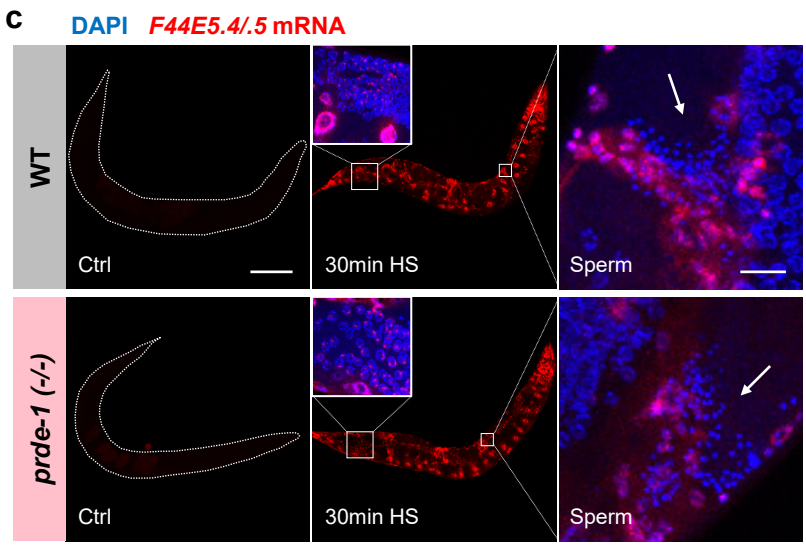

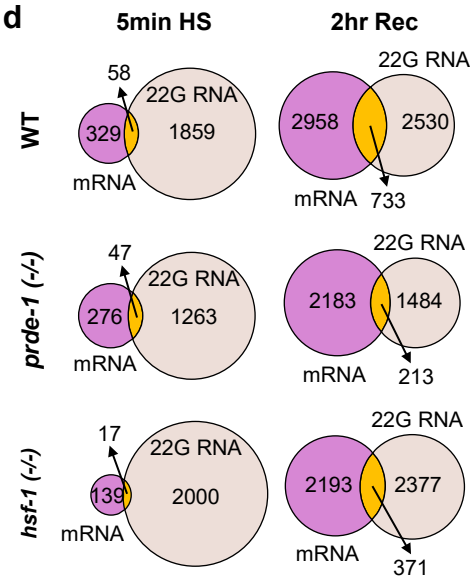

Supplementary Figure 2. piRNAs target *hsp* mRNAs expressed in the germline upon heat shock to generate 22G-RNAs.

a. Representative micrographs of projected confocal Z-sections of regions (Gonad, TZ, and Pachytene) showing RNA Fluorescence *in situ* hybridization (RNA FISH) of *hsp-70 (C12C8.1)* in WT animals. Red: *hsp-70 (C12C8.1)* mRNA. Blue: DNA staining with DAPI. Similar to Fig 1b, c. Scale bars: 50 µm (Gonad) and 3 µm (TZ, Pachytene).

b. *bath-45* immunoprecipitated with PRG-1 in non-heat shocked animals serving as a positive control for RIP experiments in Fig 1e. Bars: mean value. Error bars: standard error. n = 4 biologically independent experiments. Statistical analysis: two-tailed unpaired t-test.

c. Representative micrographs of projected confocal Z-sections showing RNA FISH of *hsp-70 (F44E5.4/.5)* mRNA in WT and *prde-1* animals upon non heat shock (Ctrl) or heat shock. Note lack of expression in sperm. Compare with 22G-RNA expression in Fig 1h. Red: *hsp-70 (F44E5.4/.5)* mRNA. Blue: DAPI stained DNA. Scale bars: 100 µm (Ctrl, 30min HS) and 10 µm (Sperm).

d. Venn diagrams showing overlap between differentially expressed mRNAs and 22G-RNAs upon 5 minutes heat shock, and for 2 hours recovery from heat shock in WT and mutant backgrounds.

Suppl. Figure 3

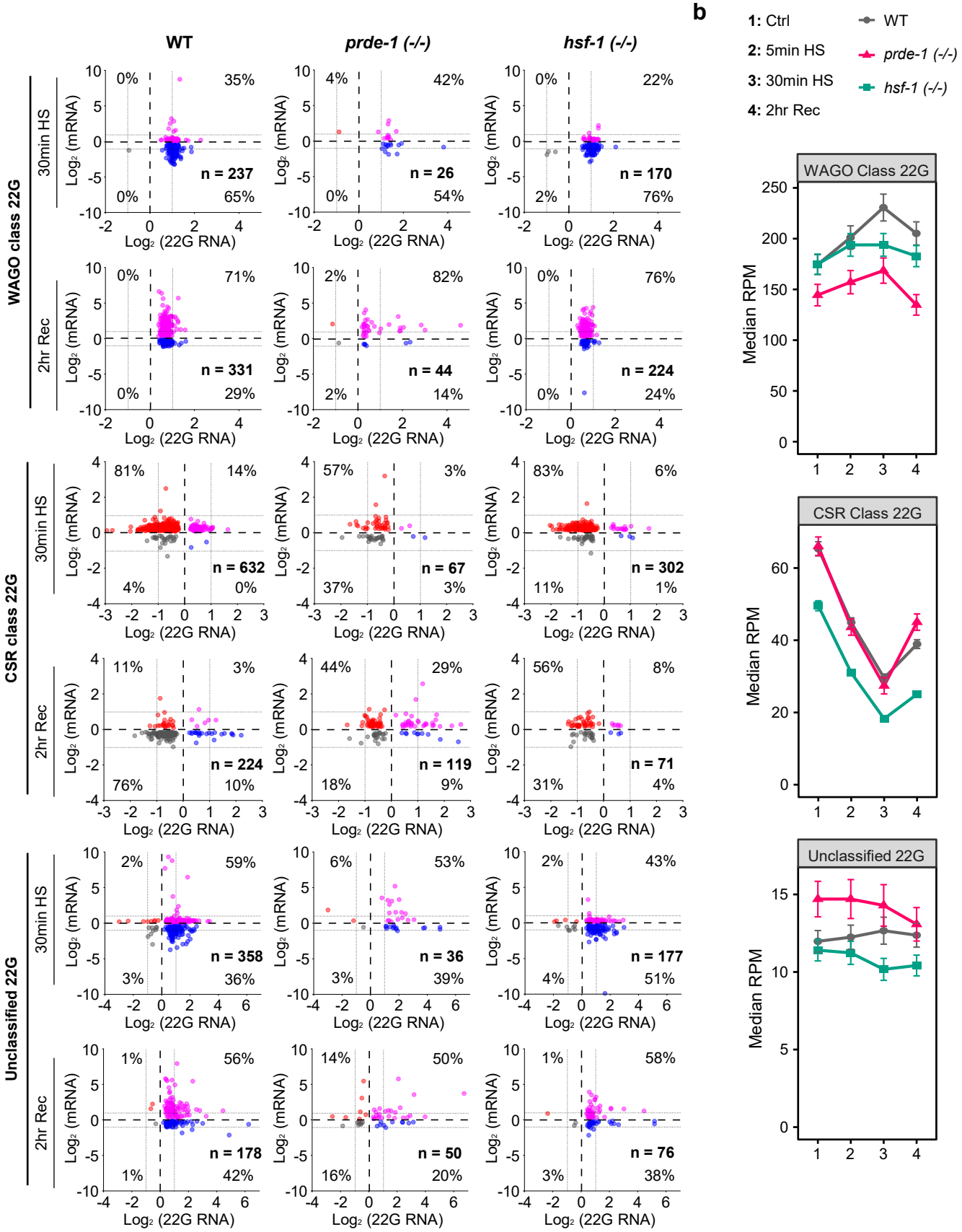

Supplementary Figure 3. piRNA-dependent WAGO and CSR-1 22G-RNAs and unclassified 22G-RNAs are templated from genes differentially expressed upon heat shock.

a. Scatter plot comparing the $\log_2$ fold-changes in WAGO class, CSR-1 class, and unclassified 22G-RNAs and complementary mRNAs in WT, *prde-1,* and *hsf-1*, upon 30min heat shock, and 2 hours recovery from heat shock. Number of mRNAs/category shown, and the % of mRNA in each quadrant of scatter plot shown.

b. Normalized expression (RPM) of WAGO and CSR-1 interacting 22G-RNAs, and unclassified 22G-RNAs in WT, *prde*-1, and *hsf-1* mutants. Y-axis: Expression (RPM). X-axis: Treatments (see top legend).

Suppl. Figure 4

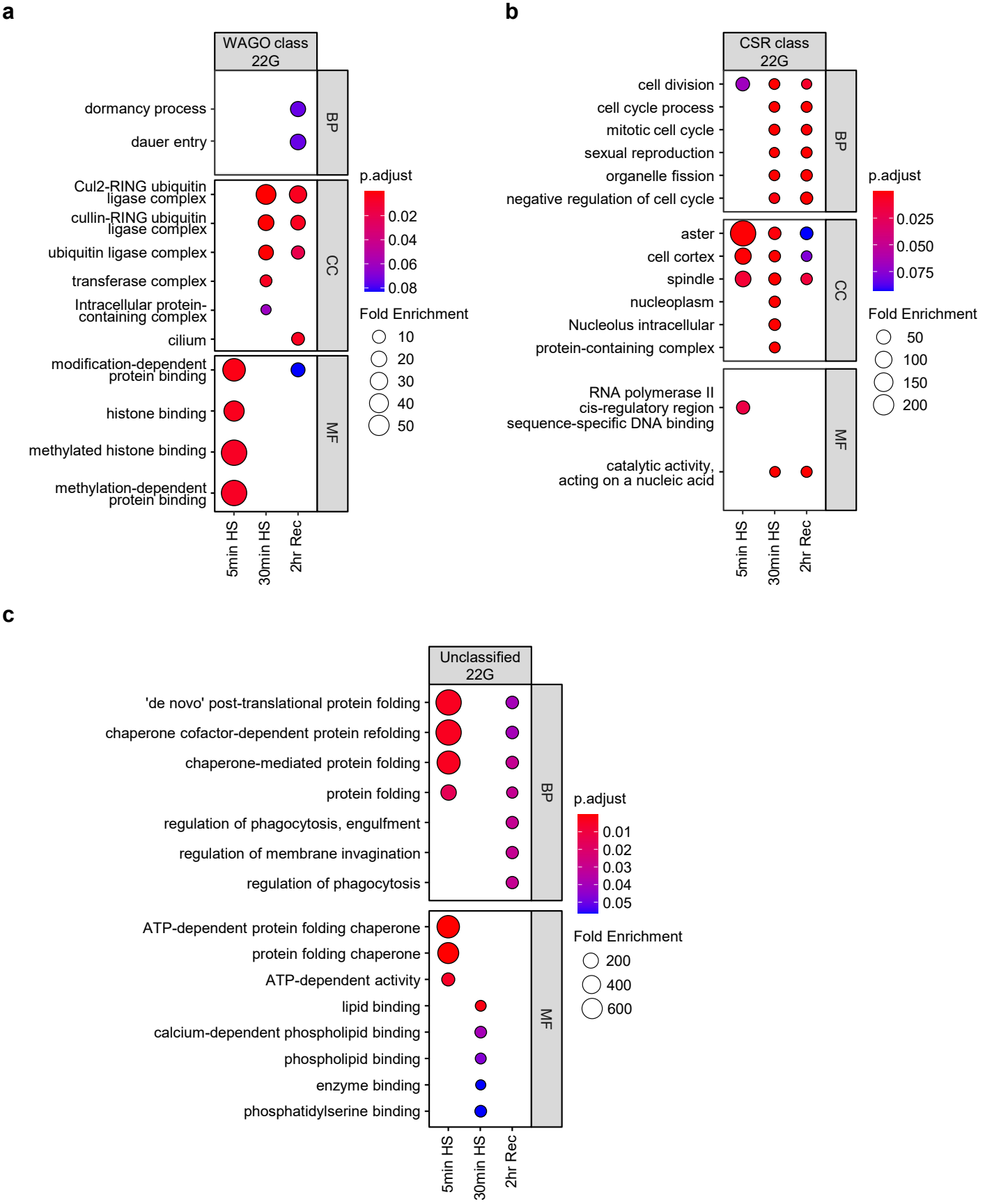

Supplementary Figure 4. 22G-RNAs produced upon heat shock target specific categories of mRNAs.

a-c. Gene Ontology analysis for **(a)** WAGO, **(b)** CSR-1, and **(c)** Unclassified 22G-RNA targets in WT animals across the different treatment conditions. All *hsp* genes are targets of unclassified 22G-RNAs (see Suppl. Table 4).

Suppl. Figure 5

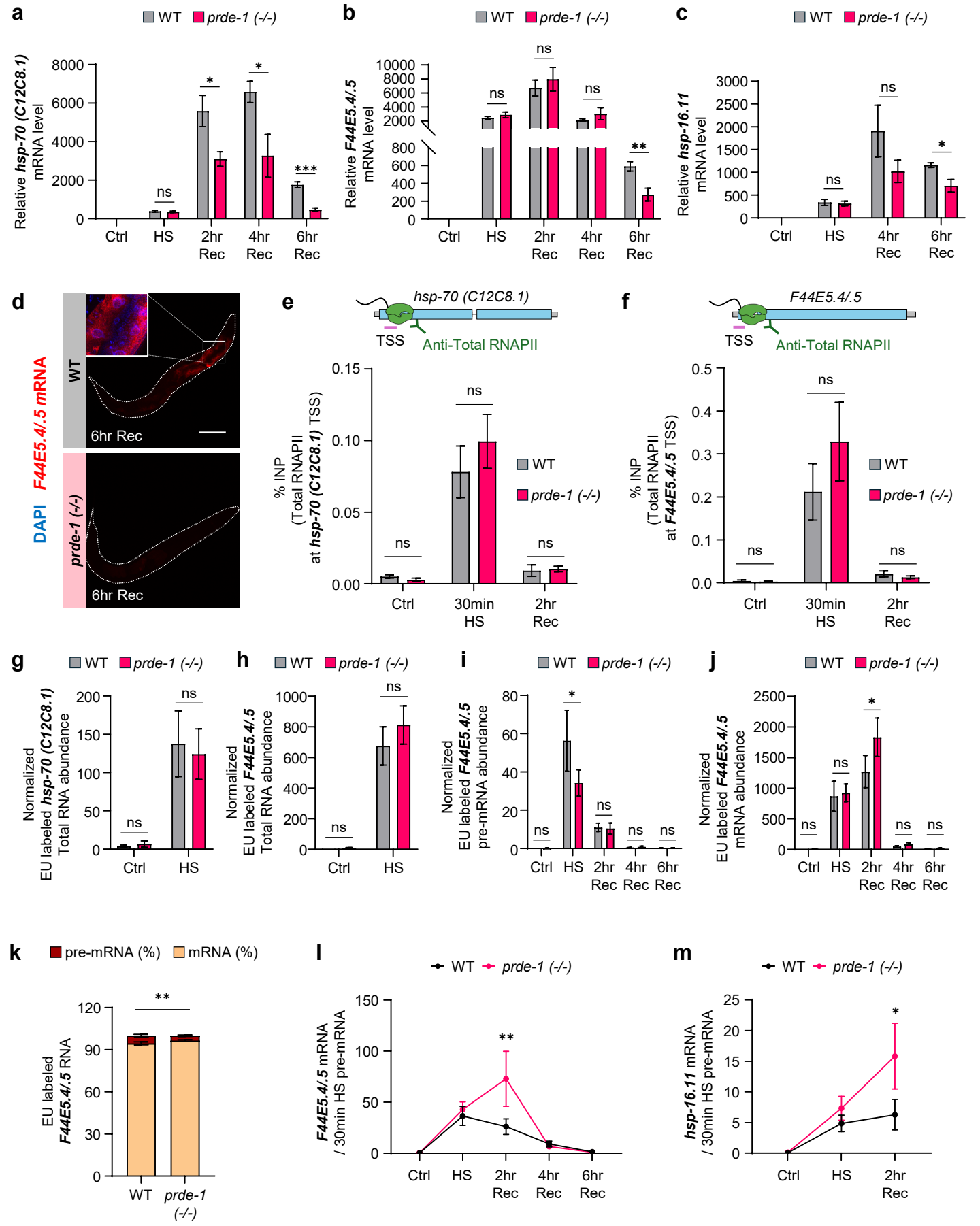

Supplementary Figure 5. The piRNA pathway protects *hsp* mRNAs persistence

a-c. RT-qPCR of relative fold change of *hsp-70s* (*C12C8.1* and *F44E5.4/.5*) and *hsp-16.11* mRNAs levels measured upon heat shock and recovery. mRNA values were normalized to *pmp-3* and shown relative to control (non-heat shocked) animals of each strain. Bars: mean value. Error bars: standard error. n = 3-13 biologically independent experiments. Statistical analysis: two-tailed unpaired t-test.

d. Representative micrographs of projected confocal Z-sections showing RNA FISH of *hsp-70 (F44E5.4/.5)* mRNA in WT and *prde-1* animals after 6 hours following heat shock. Red: *hsp-70 (F544E5.4/.5)* mRNA. Blue: DNA staining with DAPI. Scale bars: 100 μm

e, f. Total RNA polymerase II levels at *hsp* genes. **Top**: Schematic of *hsp-70 (C12C8.1* and *F44E5.4/.5)* gene, and region probed Transcription Start Site (TSS). **Bottom**: ChIP-qPCR showing fold enrichment over input. Y-axis: % ChIP input. X-axis: Treatments. Bars: mean value. Error bars: standard error. n = 3-4 biologically independent experiments. Statistical analysis: 2-way ANOVA.

g, h. Total nascent RNA abundance. EU-labeled **(g)** *hsp-70 (C12C8.1)* and **(h)** *hsp-70 (F44E5.4/.5)* RNA abundance. Y-axis: Normalized abundance. X-axis: Treatments. Bars: mean value. Error bars: standard error. n = 10-12 biologically independent experiments. Statistical analysis: 2-way ANOVA.

i, j. EU-labeled *hsp-70 (F44E5.4/.5)* **(i)** pre-mRNA and **(j)** mRNA abundance. Y-axis: Normalized abundance. X-axis: Treatments. Bars: mean value. Error bars: standard error. n = 5-13 biologically independent experiments. Statistical analysis: 2-way ANOVA.

k. Percentages of *hsp-70 (F44E5.4/.5)* pre-mRNA and mRNA in total EU-labeled RNA after 30min heat shock. Bars: mean value. Error bars: standard error. n = 13 biologically independent experiments. Statistical analysis: two-tailed unpaired t-test.

l. EU-labeled spliced *hsp-70 (F44E5.4/.5)* mRNAs produced from the nascent EU-labeled unspliced *hsp-70 (F44E5.4/.5)* pre-mRNA. Y-axis: Relative abundance. X-axis: Treatments. Line graph: mean value. Error bars: standard error. n = 5-14 biologically independent experiments. Statistical analysis: 2-way ANOVA.

m. EU-labeled spliced *hsp-16.11* mRNAs produced from the nascent EU-labeled unspliced *hsp-16.11* pre-mRNA. Y-axis: Relative abundance. X-axis: Treatments. Line graph: mean value. Error bars: standard error. n = 6-8 biologically independent experiments. Statistical analysis: 2-way ANOVA.

Suppl. Figure 6

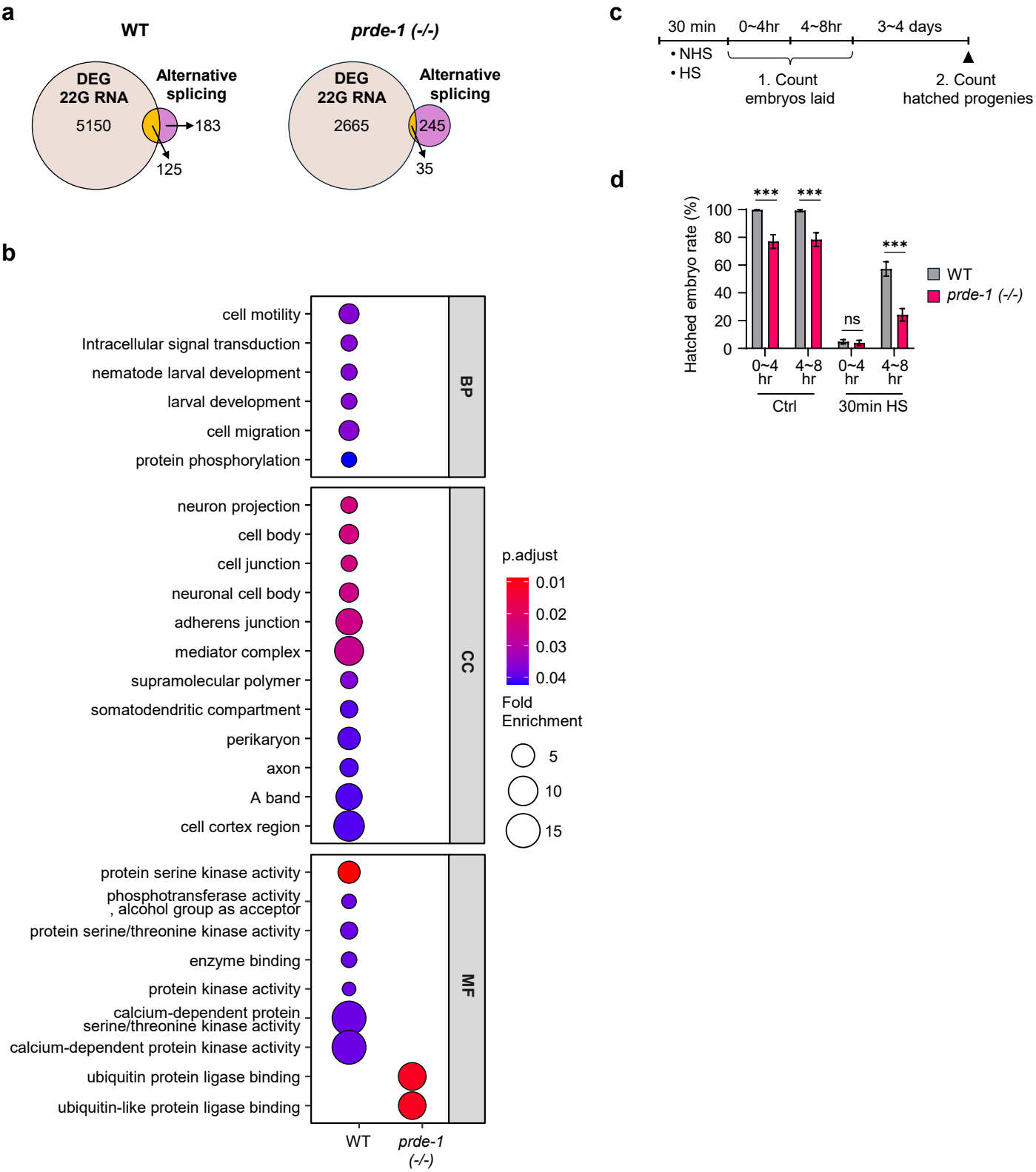

Supplementary Figure 6. Alternative splicing is affected in piRNA deficient (*prde-1*) animals.

a. Venn diagrams showing overlap between differentially expressed AS mRNAs and 22G-RNAs upon 30 minutes heat shock in WT and *prde-1* animals.

b. Gene Ontology analysis (p.adj <0.05) for AS mRNAs in WT and *prde-1* animals.

c, d. (c) Experiment schematic to assess recovery of fecundity in WT and *prde-1* animals after heat shock. NHS: non-heat shock. HS: heat shock. **(d)** Percentage of hatched embryos that laid over time during recovery from HS. Bars: mean value. Error bars: standard error. n = 7 biologically independent experiments. Statistical analysis: 2-way ANOVA.

Suppl. Figure 7

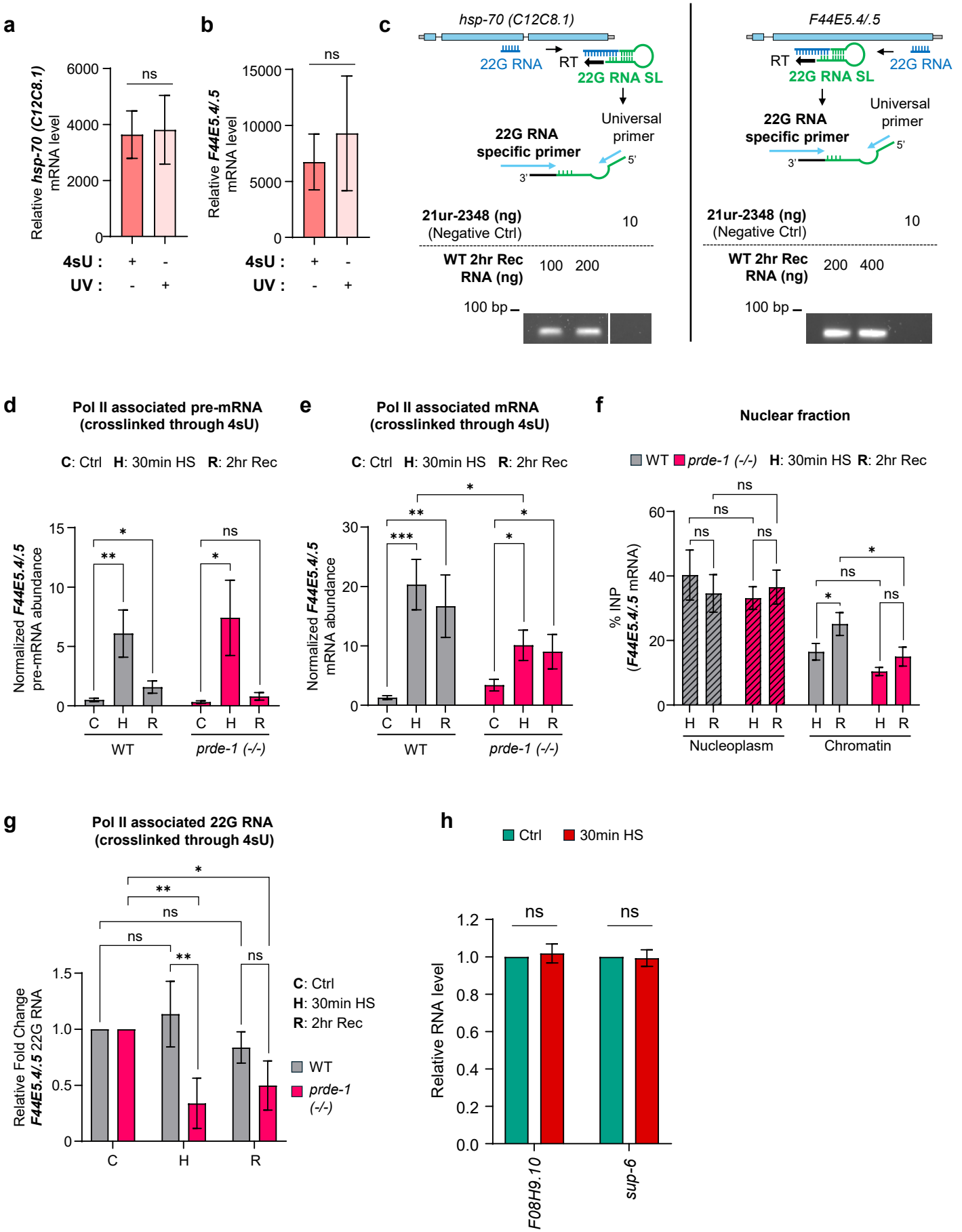

Supplementary Figure 7. 22G-RNAs associate with RNA Polymerase II and nascent *hsp* transcript to alter splicing.

a, b. 4sU treatment does not impair *hsp-70* expression. **(a)** *hsp-70 (C12C8.1)* mRNA and **(b)** *hsp-70 (F44E5.4/.5)* mRNA expressed upon heat shock in the presence and absence of either 4sU do not differ (UV exposure alone was used as comparison). Relative mRNA levels shown. mRNA values were normalized to *pmp-3* and shown relative to 4sU and UV-treated non-heat-shocked WT (value=1, not shown). Y-axis: Relative mRNA. X-axis: Treatment. Bars: mean value. Error bars: standard error. n = 3 biologically independent experiments. Statistical analysis: two-tailed unpaired t-test.

c. Stem loop RT-qPCR to amplify 22G-RNAs. **Top:** Cartoon depicting the 22G-RNA that was assayed, and complementary region on *hsp-70*. Universal primer, and 22G-RNA specific primers shown. **Bottom:** Representative agarose gel showing specificity. Different concentrations of total RNA containing 22G-RNAs were used to assess primer efficiency, and synthetically generated 21ur-2348 oligonucleotides were used as a negative control. See Materials and Methods for details. (expected PCR product size: 69bp)

d, e. Modified PAR-CLIP. Amounts of *hsp-70 (F44E5.4/.5)* **(d)** pre-mRNA and **(e)** mRNA that cross-linked to, and immunoprecipitated with Pol II normalized to *pmp-3* amounts. Y-axis: Normalized or relative abundance. X-axis: Treatment conditions (see top legend). Bars: mean value. Error bars: standard error. (d) n = 8-12 biologically independent experiments. Statistical analysis: two-tailed unpaired t-test; (e) n = 9-14 biologically independent experiments. Statistical analysis: two-tailed unpaired t-test (within strain) and 2 way-ANOVA (between strains).

f. Nuclear fractionation to assess amounts *hsp-70 (F44E5.4/.5)* RNA fate. Fold enrichment over input (nuclei) of *hsp-70 (F44E5.4/.5)* mRNA in respective fractions. Y-axis: % input (total nucleus). X-axis: Nuclear fraction, strain and treatment. Bars: mean value. Error bars: standard error. n = 9-10 biologically independent experiments. Statistical analysis: 2 way-ANOVA (within each fraction).

g. Amounts of *hsp-70* (*F44E5.4/.5*) 22G-RNA that cross-linked to, and immunoprecipitated with Pol II normalized to *pmp-3* amounts in the modified PAR-CLIP assay. Y-axis: Normalized abundance. X-axis: Treatments. Bars: mean value. Error bars: standard error. n = 4-6 biologically independent experiments. Statistical analysis: 2-way ANOVA.

h. Two other U1 RNA levels assessed upon heat shock. RT-qPCR of relative fold change in WT animals. Values normalized to *pmp-3* mRNA values and shown relative to non-heat-shock levels. Y-axis: Relative RNA levels. X-axis: U1RNAs. Bars: mean value. Error bars: standard error. n = 3 biologically independent experiments. Statistical analysis: 2-way ANOVA.

Suppl. Figure 8

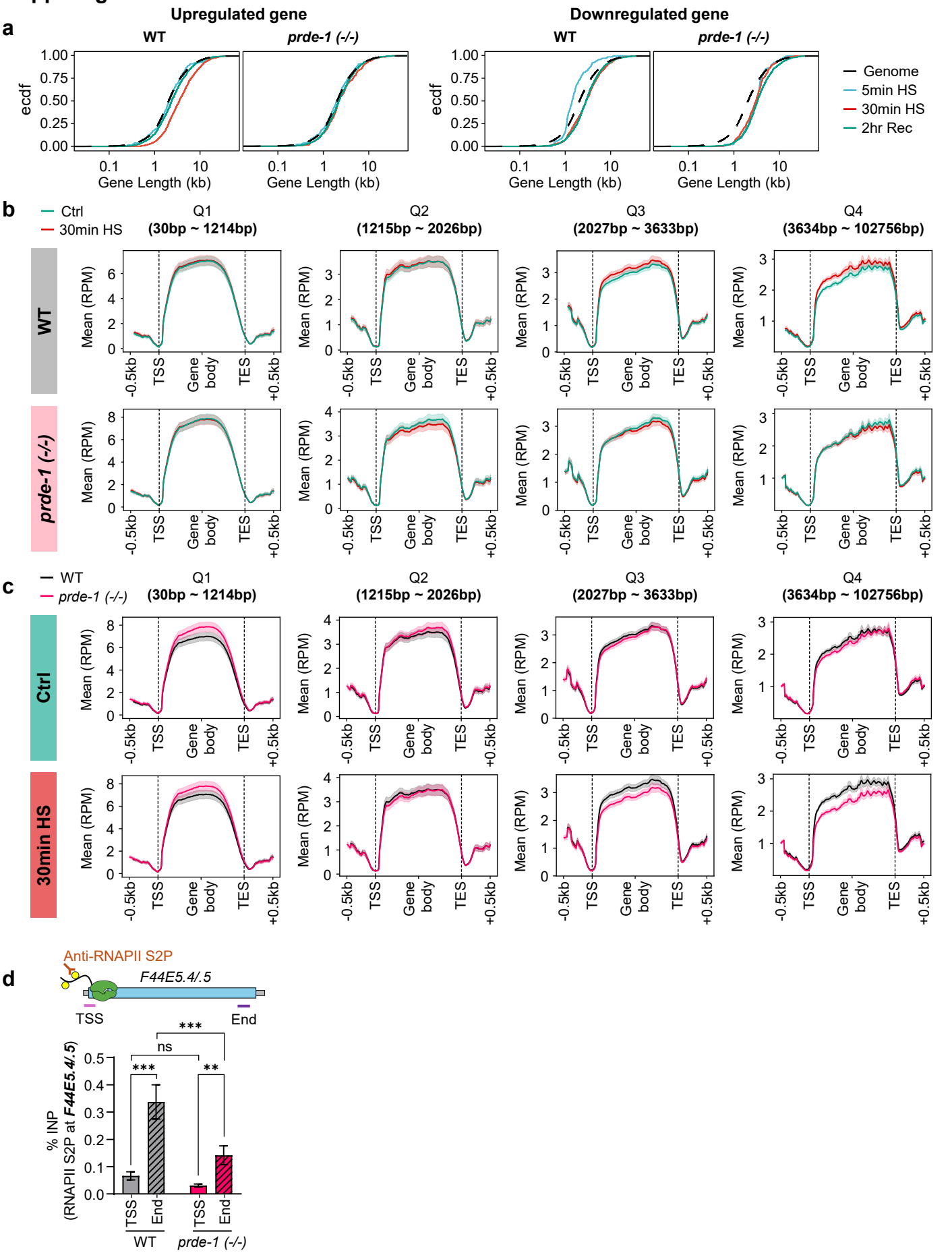

Supplementary Figure 8. piRNA pathway affects gene expression in a a gene-length dependent manner.

a. Empirical Cumulative Distribution Function (ECDF) plots, to visualize the proportion of gene expression values (mRNA-seq) as a function of gene lengths. Expression values of genes significantly upregulated and downregulated upon 30min heat shock (p.adj <0.05) in wild-type (WT) and *prde-1* are plotted. Y-axis: Cumulative proportion of reads. X-axis: Gene lengths. **Top:** Strain names and differential expression. Note bias towards increased gene lengths in WT, but not *prde-1* upregulated genes, but similar bias towards long genes in all downregulated genes.

b, c. Metagene plot showing mRNA expression (mRNA-seq) stratified by gene length compared between control and upon 30 min. heat shock, **(b)** within strains, and **(c)** between strains.

d. Elongating RNA polymerase II (anti-S2P) levels at *hsp* genes. **Top**: Schematic of *hsp-70* (*F44E5.4/.5*) gene, and regions probed: Transcription Start Site (TSS) and distal regions (3') of *hsp-70* (*F44E5.4/.5*). **Bottom:** ChIP-qPCR showing fold enrichment over input. Y-axis: % ChiP input. X-axis: Strain, and region assayed. Bars: mean value. Error bars: standard error. n = 8 (TSS) and 4 (End) biologically independent experiments. Statistical analysis: 2 way-ANOVA.

Suppl. Figure 9

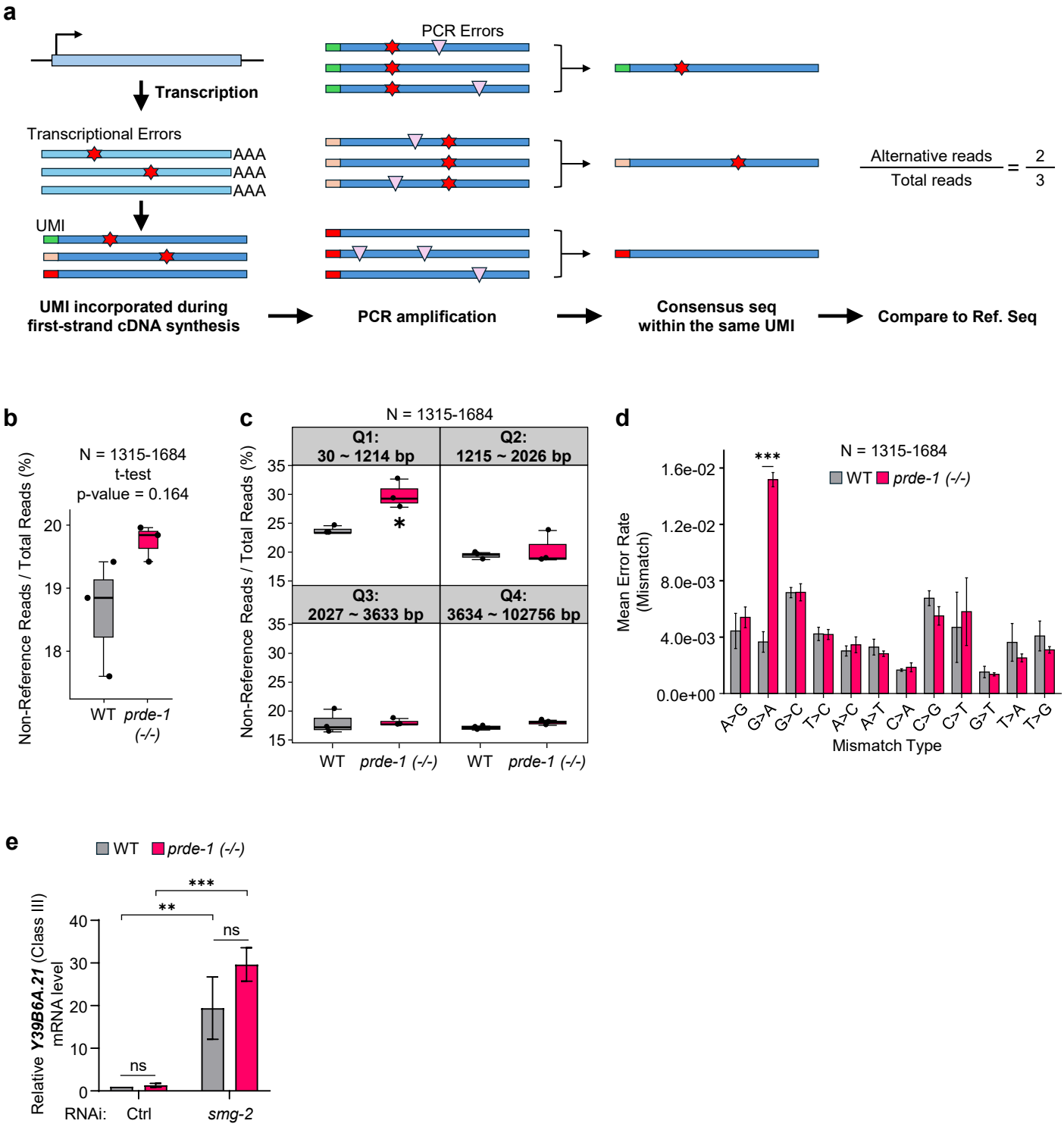

Supplementary Figure 9. piRNAs protect transcript fidelity.

a. Schematic of UMI labeling: mRNAs from wild-type and *prde-1* animals were isolated (some mRNA molecules, but not all, presumably contain errors introduced during transcription or splicing). mRNAs were labelled with UMIs during first-strand cDNA synthesis. UMI-labelled mRNAs were PCR amplified. This process also leads to the generation of PCR-based errors. The PCR-generated errors were distinguished from original errors in the mRNA by generating a consensus of UMI families. These consensus sequences were aligned to the *C.elegans* reference, mismatches identified, and the number of mRNA molecules that contained this mismatch/total number of mRNAs that mapped to that region (gene) were calculated to generate an error rate.

b. Percentage of variant-containing mRNA molecules in wild type and *prde-1* mutants (as identified by HaplotypeCaller and SnpEff). Y-axis: % variants. X-axis: Strain. Total variant containing sites=1315-1684. Approximately 3.71 x 10^7 individual mRNAs analyzed. Boxplots: median value depicted. Error bars: standard error. Statistical analysis: two-tailed unpaired t-test.

c. Percentage of variants among total variant-containing mRNA molecules expressed from genes of different lengths in wild type and *prde-1* mutants (variants identified by HaplotypeCaller and SnpEff). Q1-Q4: Genome divided into quantiles by gene length, as in Suppl. Fig 8b, c (gene lengths in bp). Y-axis: % variants. X-axis: Strain. Total variant containing sites=1315-1684. Boxplots: median value depicted. Error bars: standard error. Statistical analysis: two-tailed unpaired t-test.

d. Mean mismatch rates amongst variant-containing mRNA molecules (variants identified by HaplotypeCaller and SnpEff). Y-axis: Mean error rate (number of mismatch reads per total reads with variants). X-axis: Mismatch. Total variant containing sites=1315-1684. Approximately 3.71 x

10^7 individual mRNAs analyzed. Bars: mean value. Error bars: standard error. Statistical analysis: two-tailed unpaired t-test.

e. NMD-related gene expression levels in WT and *prde-1* animals on Ctrl (L4440) and *smg-2* RNAi (RT-qPCR: relative fold change). *Y39B6A.21* (Class III) expression values normalized to *eft-3* mRNA values and shown relative to wild-type Control RNAi-treated animals. Note *that smg-2 leads to a similar increase in mRNA levels in both wild-type* and *prde*-1. Y-axis: Relative RNA levels. X-axis: RNAi-treatment. Bars: mean value. Error bars: standard error. n = 4 biologically independent experiments. Statistical analysis: 2-way ANOVA.

C. ELEGANS STRAINS AND GROWTH CONDITIONS

C. elegans used in all experiments are listed in Method Table 1. Strains were obtained from the *Caenorhabditis Genetics Center* (CGC, Twin Cities, MN), generated in the Prahlad laboratory, or generated by SunyBiotech (Suzhou, Jiangsu, China). All crossed worms were verified by genotyping. The primers used in genotyping are listed in Method Table 2.

All strains were maintained at 20°C on nematode growth media (NGM) plates. NGM plates were prepared by pouring 8.9 ml of autoclaved liquid NGM per 60 mm plate. NGM was allowed to solidify at room temperature (RT) for 2 days, seeded with 300 µl OP50 *E. coli* (O.D = 1.8-2.0), and dried at RT for no more than 2 days. Population densities were matched based on growth rate of the strains. To maintain healthy continuously growing populations, 10-15 animals at larvae stage 4 (L4) were passaged onto a new plate every 4 days. For experiments, day-one adult animals were used. These were generated either by picking L4-stage worms and harvesting them 24-24 hrs later, or by bleach-hatching and collecting day-one adult worms 82-84 hrs later, depending on experimental requirements.

HEAT SHOCK

Worms were exposed to acute heat stress as previously described in Das et al., elife 2020[1]. Briefly, NGM plates containing day-one adults were sealed with parafilm and immersed in a water bath pre-warmed to 34°C for different durations as mentioned. For recovery experiments, NGM plates were incubated in a 20°C incubator immediately after heat shock and harvested after specific times mentioned in the experiments.

RNA SEQUENCING

RNA Library Preparation

26 For RNA-sequencing, three independent biological replicates of each strain and each treatment
27 were harvested and processed as described. For each sample/treatment, approximately 200
28 L4-stage worms were transferred to OP50 plates. After 26-27hrs, worms from two plates per
29 condition [non-heat shock (NHS), 5min HS, 30min HS, and 30min HS + 2hr Rec] were collected
30 in nuclease-free water. Total RNA was extracted using the Mirvana miRNA Isolation Kit
31 (Invitrogen; Cat #AM1560). Genomic DNA in the sample was removed using Turbo DNA-free Kit
32 (Invitrogen; Cat #AM1907). RNA was separated by size into mRNA (>200 nt) and small RNA
33 (<200 nt). Small RNA samples were treated with 10U RppH (NEB; Cat #M0356S) at 37°C for 30
34 min, then purified using the Zymo RNA Clean & Concentrator kit (Zymo Research; Cat #R1015).
35 RNA concentrations were measured with a Qubit 4 fluorometer (Thermo Scientific). mRNA
36 libraries were prepared using the KAPA mRNA Hyperprep kit (Roche; Cat #08098123702);
37 small RNA libraries were prepared using the Illumina TruSeq Small RNA Library Preparation kit
38 (Illumina; Cat #RS-200), following manufacturer's protocol.
39
40 ***Small RNA analysis***
41 Small RNA data was analyzed using the tinyRNA[2] (v1.50) pipeline with its default configuration.
42 The process included adapter trimming and quality filtering with fastp[3], followed by genome
43 alignment to the *C. elegans* genome (release WS279) using Bowtie[4]. An additional setting,
44 counter_decollapse: True, was specified to generate decollapsed SAM files.
45 The module tiny-count was used to count the different types of small RNA according to the
46 selection rules specified in the following table.

Select for...	with value...	Classify as...	Hierarchy	Overlap	Strand	5'End Nucleotide	Length
Class	risiRNA	rRNA	1	Partial	both	all	all

Select for...	with value...	Classify as...	Hierarchy	Overlap	Strand	5'End Nucleotide	Length
Class	miRNA	miRNA	2	5'Anchored, 0, 4	sense	all	all
Class	piRNA	piRNA	2	5'Anchored	sense	all	18-21
Class	CSR	CSR Class 22G	3	Partial	antisense	G	21-23
Class	WAGO	WAGO Class 22G	3	Partial	antisense	G	21-23
Class	ALG	ALG Class 26G	3	Partial	antisense	G	26
Class	ERGO	ERGO Class 26G	3	Partial	antisense	G	26
Class	ALG	ALG target 22G	3	Partial	antisense	G	21-23
Class	ERGO	ERGO target 22G	3	Partial	antisense	G	21-23
Class	unk	unclassifed 22G	3	Partial	antisense	G	21-23
Class	unk	unclassifed siRNA	4	Partial	both	all	21-24

The read counts obtained from tiny-count were used to generate genome-wide coverage profiles for the 22G-RNAs and piRNA. The coverage was normalized as Read per million (RPM) and output as BigWig (bw) files using rtracklayer[5]. Differential Expression was computed by using a modified version of tyny.deseq.r, the R module was adjusted to remove the ribosomal RNA (rRNA) from the analysis, and to calculate the gene expression in RPM in addition to

53 DESeq normalized counts. Changes in expression were presented as log_2 fold-change, and
54 genes with an adjusted p-value of <0.05 (after correction with Benjamini & Hochberg)[6], were
55 considered significant.
56
57 ***mRNA seq analysis***
58 RNA-seq samples were analyzed and processed using the nf-core/rnaseq (v3.12.0) pipeline,
59 which was executed with Nextflow[7] (v22.10.6). Sequence quality was assessed with FastQC
60 [8](v0.11.9), and low-quality reads, and adapters were removed using Trimmomatic[9] (v0.67). The
61 processed reads were then aligned to the *C. elegans* genome (WBcel235, Ensembl release
62 111) with STAR[10] (v2.7.9a) using default settings. Alignments were quantified against the
63 WBcel235 annotation with Salmon (v1.9.0). Alignment quality control was performed with
64 Qualimap[11] (v2.2.2) and RSeQC[12] (v3.0.1).
65
66 ***Differential Expression***
67 Differential expression analysis was performed between RNA-seq samples using **DESeq2** with
68 the **Wald test**. Expression changes were presented as log2 fold-change. Genes with an
69 adjusted p-value <0.05, following correction with the **Benjamini & Hochberg**[6] method, were
70 considered significantly differentially expressed.
71
72 ***Analysis of Alternative Splicing Events***
73 To identify differential alternative splicing events, RNA-seq data were re-processed using the nf-
74 core/rnasplice (v1.0.4) workflow. This pipeline was executed with Nextflow (v23.10.0) and relied
75 on reproducible software environments from Bioconda and Biocontainers.
76
77 Within the rnasplice pipeline two modules were used to detect differential splicing and calculate
78 the Percent Spliced-In (PSI) for each event, SUPPA2[13] (v2.3) and rMATS (v4.1.2)., Splicing

events were considered significant if the absolute difference in PSI (dPSI) between the 30 minutes heat shock and control conditions had a p-value <0.1.

Formula : $\boldsymbol{\Psi} = \sum(\boldsymbol{TPMinclusion}) + \sum(\boldsymbol{TPMexclusion}) \sum(\boldsymbol{TPMinclusion})$ [13]

Pearson's Chi-squared test with Yates' correction was used to determine if the number of up- or down-regulated splicing events during heat shock differed between the N2 and PRDE1 strains (p-value <0.05).

Differential Transcript Usage (DTU) analysis was performed using SUPPA2. First, the usage of transcripts (isoforms) was tested for significant differences between conditions. Isoforms with a p <0.1 were considered significant. For analysis and visualization, the average Percent Spliced In (PSI or Ψ) value for each isoform was calculated across the biological replicates within each condition. The resulting list of PSI per isoforms was then filtered to retain only those occurring in genes previously identified as differentially expressed (DEGs). Student t-test was used to compare the means between the conditions at significance level p <0.05.

Formula: $\boldsymbol{PSI_i} = (\boldsymbol{TPM_i})/(\boldsymbol{\Sigma_(j = 1)\hat{}n\ TPM_j})$ [13]

Gene Ontology

Gene Ontology analysis was performed by using Over Representation Analysis (ORA), with the R package ClusterProfiler[14,15]. GO annotations for *C. elegans* were obtained from R package org.Ce.eg.db: Genome wide annotation for Worm[16] (version 3.18.0). Ontology terms enriched with an adjusted p-value <0.05 or <0.1 (Benjamini & Hochberg)[6] were considered significant. Fold-Enrichment was calculated as the ratio of the frequency of input genes annotated in a GO term to the frequency of all genes annotated to that term[14].

Data Visualization

105 The metaprofiles were generated using Deeptools[17] (v3.56) by normalizing the coverage by
106 RPM per bp) and then modified to plot them using R.
107
108 Venn diagrams were generated using the Eulerr[18] package (v.7.0.2) in R[18]. Additional plots were
109 generated using ggplot2 (v.3.5.1)[19] .
110
111 **RNA FISH**
112 ***mRNA FISH***
113 RNA FISH was performed as previously described[20]. Probes were designed against mRNA
114 according to the Biosearch Technologies website, and consisted of 25-35 11bp sequences that
115 were complementary to the *hsp-70s (C12C8.1* and *F44E5.4/.5)* mRNA. For mRNA FISH, about
116 20 day-one adult worms were harvested in 1x PBS and fixed in 4% paraformaldehyde (Electron
117 Microscopy Science; Cat #50-980-487) for 45 mins. After two washes with 1x PBS, worms were
118 permeabilized in 70% ethanol at 4°C for 24-26 hrs. Worms were washed with Stellaris Buffer A
119 (Biosearch Technologies, Cat # SMF-WA1-60) and incubated at 37°C for 16 hrs in hybridization
120 buffer (Cat #SMF-HB1-10) containing 0.2 mM FISH probes targeting *hsp-70s (C12C8.1* and
121 *F44E5.4/.5)* mRNA. After washing three times with pre-warmed Wash Buffer A and one time
122 with Wash Buffer B (Biosearch Technologies, Cat # SMF-WB1-20), worms were mounted in
123 Vectashield with DAPI (Vector Laboratories; Cat #H-1200-10). Imaging was performed using a
124 Leica TCS SPE Confocal Microscope with 20x dry and 63x oil objectives, and LAS AF software.
125
126 ***22G RNA FISH***
127 For 22G-RNA FISH, animals were processed as described above for mRNA FISH.
128 Fluorescence conjugated probes targeting 22G-RNAs were purchased from IDT, and were
129 complementary to one of the most abundant 22G-RNAs identified by sRNA-seq (hence they
130 were in the sense direction as mRNA, and could not hybridize to mRNA). 0.2 μM FISH probe

131 targeting *F44E5.4/.5* 22G RNA was used per slide. The sequence of the probe is in Method
132 Table 3.
133
134 **AUXIN-INDUCIBLE DEGRADATION (AID) TREATMENT**
135 Auxin plates were prepared at a final concentration of 4 mM by adding indole-3-acetic acid (Alfa
136 Aesar; Cat #A10556), dissolved in ethanol at 400 mM, to autoclaved NGM that had cooled to
137 approximately 55°C prior to pouring. NGM plates with ethanol served as controls. Plates were
138 dried at RT for 2 days, then for 2 more days after seeding with 300 µl OP50 (O.D = 1.8-2.0).
139 About 20 day-one adults were transferred to OP50-seeded auxin or ethanol plates and
140 incubated at 20°C for 4 hrs. Worms were then either not heat shocked (NHS) or subjected to
141 heat shock (HS) for 30mins at 34ºC and processed for FISH as above.
142
143 **IMMUNOSTAINING**
144 Immunostaining of dissected gonad was performed as previously described[20] . 10-15 day-one
145 adults were picked into 15 µl 1x PBS on a cover glass (Leica Biosystem; Cat #3800105) and
146 dissected with a surgical blade #11. Dissected worms were fixed in 4% paraformaldehyde for 6
147 mins. A charged slide (Epredia; Cat #4951PLUS-001) was placed over the cover glass, then
148 quickly transferred onto a metal block that had been cooled with dry ice for over 10mins. After
149 quickly removing the cover glass, samples were post-fixed in 100% methanol pre-chilled at
150 −20°C for 2mins, washed in 1x PBST (1x PBS with 0.1% Tween-20), and then blocked in 1x
151 PBST with 0.5% BSA for 1 hr. Samples were incubated at 4°C overnight with Mouse anti-FLAG
152 M2 (Sigma-Aldrich, Cat #F3165-1MG), diluted 1:2,000 in 1x PBST. Following washing, samples
153 were incubated at RT for 2 hrs with Donkey anti-Mouse Alexa Fluor 488 (Invitrogen; Cat
154 #A32766), diluted 1:500 in 1x PBST. After washing, samples were mounted in the Vectashield
155 with DAPI and imaged.
156

157 **RNA INTERFERENCE (RNAi)**

158 RNAi experiments were conducted using the standard feeding RNAi methods. Bacterial clones
159 expressing the control (empty vector pL4440) construct and the dsRNA targeting
160 different *C. elegans* genes were obtained from the Ahringer RNAi library[21] , now available
161 through Source Bioscience. All RNAi clones used in experiments were sequenced for
162 verification. For RNAi experiments, RNAi bacteria with empty (pL4440 vector as control) or the
163 dsRNA-expressing plasmid were grown overnight in LB liquid culture containing ampicillin
164 (100 µg/ml) and then induced with IPTG (1 mM) for 2 hrs before seeding the bacteria on NGM
165 plates supplemented with ampicillin (100 µg/ml) and IPTG (1 mM). Bacterial lawns were allowed
166 to grow 48hr before the start of the experiment. RNAi-seeded plates were used for RT-qPCR
167 experiments to measure NMD-related gene expression, to evaluate the hatch rate of embryos,
168 and for immunoblot assays (to analyze ubiquitinylated proteins). For RT-qPCR and Western blot
169 experiments, worms were initially grown on OP50 plates for 24 hours after egg laying or
170 bleaching, respectively. Then, larvae were transferred to RNAi plates and grown for 60-62 hours
171 before harvesting. This was done to bypass the embryonic lethality of *smg-1* or *smg-2* RNAi.
172

173 **RNA ISOLATION AND QUANTIFICATION OF RNA LEVELS BY RT-qPCR**

174 RNA was extracted from 30-40-day-old adults exposed to the indicated heat shock durations
175 and recovery times. Animals were collected in 50 µl Trizol and immediately snap-frozen in liquid
176 nitrogen. Samples were thawed on ice, mixed with 200 µl Trizol, and lysed using Precellys 24
177 homogenizer. RNA was isolated from lysates with chloroform and precipitated with isopropanol
178 and glycogen. After washing with 70% EtOH, RNA pellet was dissolved in nuclease-free water
179 and treated with TURBO DNase. cDNA was synthesized using iScript cDNA synthesis kit (Bio-
180 Rad; Cat #1708891). qPCR was performed using PowerUp SYBR Green Master Mix (Applied
181 Biosystems; Cat #A25742) on a QuantStudio 3 Real-time PCR System (10 µl reaction, 96-well
182 plate).

183

184 The amounts of RNA were quantified using one of the following methods:

185 ***mRNA RT-pPCR***

186 (i) Relative quantification using the ΔΔCt method: mRNA (exon-exon junction primers), and pre-

187 mRNA (intron-exon primers) levels were computed relative to *pmp-3* (previously verified by use

188 to remain steady during heat shock)[1], which served as an internal control. For NMD-related

189 gene expression analysis, *eft-3* was used as internal control, as previously described[22]. Primer

190 locations are depicted in the Method Fig 1 below and primer sequences are in Method Table 2.

191

192 (ii) Absolute quantification using standard curves: Absolute amounts of pre-mRNA and mRNA

193 were estimated through the generation of standard curves using serial dilutions of defined

194 concentrations of *hsp-70 (C12C8.1)* and *F44E5.4/.5* mRNA, pre-mRNA, as well as *pmp-3*

195 mRNA. The mRNA and pre-mRNA used to generate each standard curve, was obtained by

196 PCR amplification from cDNA or genomic DNA extracted from whole worms, PCR amplified

197 using primers external to the primer target sites used in the experiments, gel purification, and

198 quantification using a Qubit 4 fluorometer. qPCR was conducted using 10-fold serial dilutions of

199 a known concentration of purified PCR products. The standard curves were created from the CT

200 values obtained from the dilutions (see Method Fig 1).

201 The amounts of mRNA and pre-mRNA were extrapolated derived from these curves using the

202 formula.

203 **Formula:** $\boldsymbol{Absolute\ amount\ of\ RNA = Inital\ Con. \times 10^{\left(\frac{CT\ Value - constant}{slope}\right)}}$

204 To account for differences in lysis efficiency, variations in harvesting of animals, and other

205 factors, a similar curve was calculated for *pmp-3* and the final values were normalized to *pmp*-3

206 values known to remain stable through heat shock[1].

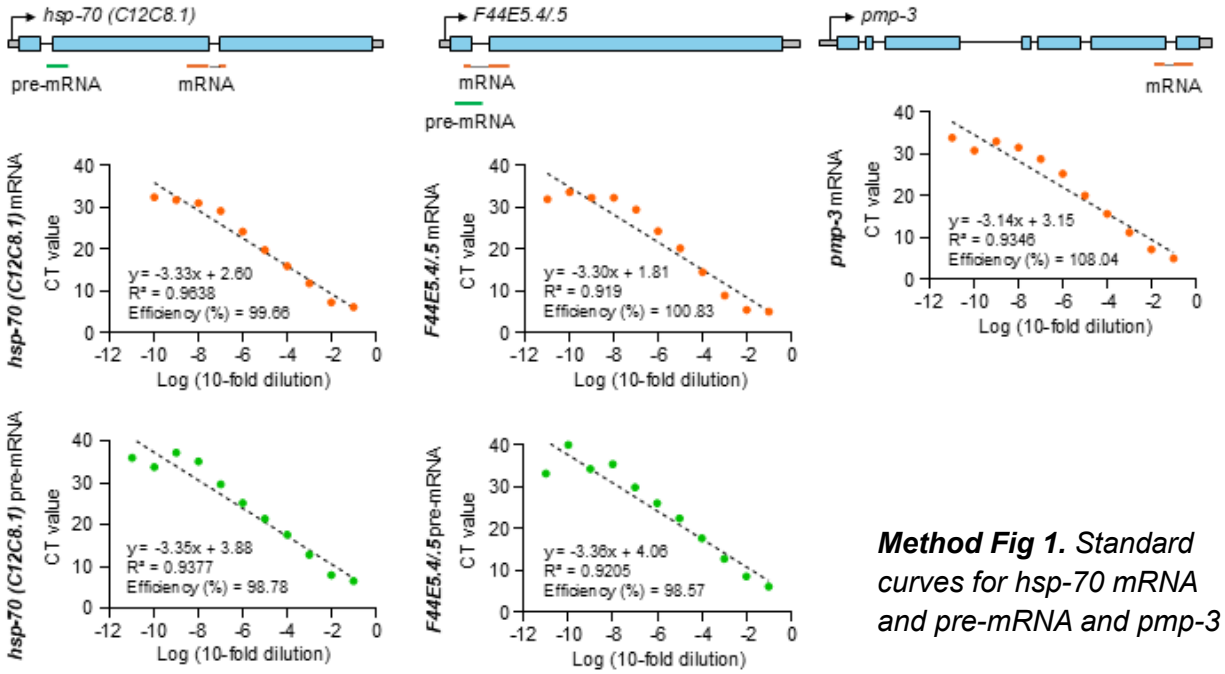

Method Fig 1. *Standard curves for hsp-70 mRNA and pre-mRNA and pmp-3*

207

208 The primers used for qPCR analysis were designed using Primer 3 software and generated by

209 Integrated DNA Technologies (See Method Table 2).

210

211 ***SMALL RNA (sRNA) RT-qPCR***

212 Small RNA qPCR was performed using stem-loop RT-qPCR by modifying published protocols[23]

213 Total RNA extracted from animals, or immunoprecipitated after 4sU treatment and RNAPII

214 immunoprecipitation (see below), incubated with 50 nM 22G RNA-specific stem loop primer at

215 70°C for 5mins, cooled on ice for ≥5 mins. cDNA was synthesized using 100U Superscript II

216 Reverse Transcriptase (Invitrogen; Cat #18064014) in 1x reaction buffer, 1U SUPERase-In

217 RNase inhibitor, and 0.5 mM dNTPs. The RT-qPCR mix included 2 µl cDNA, 0.25 µM 22G RNA-

218 specific forward primer, 0.25 μM universal reverse primer,1x PowerUp SYBR Green Master Mix.
219 Relative fold change of 22G-RNA was quantified relative to immunoprecipitated *pmp-3* using the
220 ΔΔCt method. Primer specificity was tested using a synthetic sRNA (21ur-2348). The specificity
221 of the reaction was verified by running the reaction on agarose gels. Representative gel and
222 PCR design are shown in Suppl. Fig 7c. The primer sequences are listed in Method Table 3.
223
224 **ChIP-qPCR**
225 Chromatin immunoprecipitation (ChIP) was performed as previously described[20] . Following
226 exposure to one of three conditions (NHS, 30min HS, or 30min HS + 2hr Rec), approximately
227 700 day-one adults, synchronized by bleach hatching, were harvested in 1x PBS and
228 crosslinked with 2% formaldehyde at RT for 10 mins. Crosslinking was quenched with 250 mM
229 Tris (pH 7.4) for 10 mins. Samples were washed three times in ice-cold 1× PBS containing
230 protease inhibitor cocktail (PIC; Thermo Scientific; Cat #78429) and then snap-frozen in liquid
231 nitrogen. Pellets were resuspended in 200 μl FA buffer (50 mM HEPES/KOH (pH 7.4), 150 mM
232 NaCl, 50 mM EDTA, 1% Triton X-100, 0.1% sodium deoxycholate, 0.5% sarkosyl) freshly
233 supplemented with 1 mM DTT and 1x PIC. Worms were lysed using a Precellys 24
234 homogenizer and sonicated (Bioruptor Pico; 8-10 cycles of 30sec on/off). Debris was removed
235 by centrifugation (13,500 rpm at 4°C for 5 mins). Protein A/G Magnetic Beads (20 μl per sample;
236 Thermo Scientific, Cat #88803) were washed two times with FA buffer. To eliminate non-specific
237 binding, 5 μl of beads were then added to the lysates and incubated at 4°C for 1 hr. 10% of the
238 pre-cleared lysate was kept as input, and the rest was incubated overnight at 4°C with anti-total
239 RNAPII (Diagenode; Cat #C1520004) or RNAPII s2P (Diagenode; Cat #15200005), followed by
240 3 hrs incubation with 15 μl beads. Beads were washed sequentially with low salt, high salt, LiCl,
241 and TE buffers, then eluted in 150 μl elution buffer (10 mM EDTA, 1% SDS, 0.1 M sodium
242 bicarbonate). Elutes and volume-matched inputs were de-crosslinked overnight with 0.8U
243 proteinase K (NEB; Cat #P8107S) and 160 mM NaCl. DNA was purified using

244 phenol/chloroform/isoamyl alcohol. qPCR was performed as above. All experiments were
245 expressed as % input value. The sequence of the primers used for ChIP experiments are listed
246 in Method Table 2 and depicted in Fig 3j; Suppl. Fig 5e, f, and 8d.
247
248 **RNA IMMUNOPRECIPITATION (RIP) FOLLOWED BY RT-qPCR**
249 RNA immunoprecipitation (RIP) was performed with ~700 day-one adults per condition,
250 expressing FLAG::FRG-1 (endogenous PRG-1 tagged with FLAG epitope using CRISPR/Cas9)
251 synchronized by bleach hatching. To account for the non-specific interactions of the abundant
252 *hsp* mRNA generated by heat shock, we used wild-type (N2) animals not expressing FLAG as a
253 negative control, and compared specific immunoprecipitation (IP) of PRG-1 IP to this non-
254 specific IP. RIP was conducted in the absence of cross-linking. Worms were harvested in
255 nuclease-free water, pelleted, and snap-frozen in liquid nitrogen. Worms were resuspended in
256 FA buffer with 1 mM DTT, 1x PIC, and 0.01U/µl SUPERase-In RNase inhibitor (Invitrogen; Cat
257 #AM2696), then lysed and sonicated (2 cycles of 30 sec on/off). 10% of the pre-cleared lysate
258 was kept as input, and the rest was incubated with anti-FLAG M2 (Sigma-Aldrich, Cat #F3165-
259 1MG) at 4°C for 2-3 hrs, followed by beads for 1hr. After washing, beads were eluted with
260 elution buffer containing 0.01U/µl SUPERase-In RNase inhibitor. Elutes and volume-matched
261 inputs were de-crosslinked by incubating them with 0.8U proteinase K (NEB; Cat #P8107S) at
262 45°C for 1hr. RNA was isolated using Trizol and qRT-PCR was performed as above. Because
263 we were had no reason to expect that *pmp-3* would also bind to PRG-1, and be
264 immunoprecipitated, to control for variation in harvesting, lysis, loading etc., we normalized *hsps*
265 in IP sample to *pmp-3* in the input sample using the ΔΔCt method. *bath-45*, known to interact
266 with PRG-1 was used as a positive control for the efficacy of RIP. The sequence of the primers
267 used for RIP experiments are listed in Method Table 2.
268
269 **4sU RNAPII IP qPCR**

270 All procedures for 4sU RNAPII immunoprecipitation (IP) are outlined in Fig 3a. Specifically, 4sU
271 was delivered as a liquid suspension mixed with bacterial food. The bacterial food, OP50, was
272 heat-killed to minimize its metabolism of 4-Thiouridine (4sU). To most optimally deliver 4sU
273 within a short time, about 700 day-one adult worms were rapidly collected in nuclease-free
274 water and then resuspended in S-basal containing 10mg/ml heat-killed OP50 and 4mM 4sU
275 (Sigma Aldrich; Cat #T4509). The suspension was seeded onto empty NGM plates to prevent
276 hypoxia (a critical step since *C.elegans* suspended in liquid media have a markedly different
277 heat shock response). The worms, bacteria and 4sU were allowed to dry at RT for 1hr, and
278 subjected to one of three conditions [not heat shocked (NHS), heat shocked at 34ºC for 30 mins
279 (30min HS), or heat shocked at 34ºC for 30 mins and allowed to recover for 2 hrs at 20ºC
280 (30min HS + 2hr Rec)], and then crosslinked by exposure to UV (365 nm) for 30 sec. Samples
281 were harvested in nuclease free water and snap-frozen in liquid nitrogen. Worm lysis,
282 immunoprecipitation, RNA isolation, and qRT-PCR followed the RIP-qRT-PCR protocol, using
283 anti-total RNAPII (Diagenode; Cat #C1520004) instead of anti-FLAG. To quantify mRNA and
284 pre-mRNA, absolute amounts of RNA were estimated from standard curves and normalized by
285 immunoprecipitated *pmp-3*.
286
287 **EU LABELLING OF NASCENT RNA**
288 To examine the expression patterns of nascent *hsp* genes we used a pulse-chase approach
289 using the Click-iT Nascent RNA Capture Kit (Invitrogen; Cat #C10365) according to the
290 manufacturer's instructions, to label RNA. In brief, 50 day-one adult worms were placed on an
291 OP50 bacterial lawn containing 4 mM EU and incubated at 20°C for 10 mins to preload them
292 with EU. Subsequently, the worms were incubated at 20°C (serving as controls) or underwent
293 heat shock for 30 mins at 34ºC. Control and heat shocked animals were harvested in 50 µl
294 Trizol and immediately snap-frozen in liquid nitrogen. To assess maturation of pre-mRNA to
295 mRNA, animals were allowed to recover in the absence of EU. For this, worms were

296 transferred, immediately after heat shock, from EU containing OP50 plates onto new NGM
297 plates seeded with regular OP50. The plates were then incubated at 20°C for 2, 4, or 6 hours,
298 and subsequently harvested in Trizol. RNA isolation was performed as described in the RT-
299 qPCR protocol. EU-labeled RNA was biotinylated with 0.4 mM biotin azide and purified by
300 reprecipitating. The biotinylated RNA was captured using 12 µl of streptavidin beads. cDNA
301 synthesis was carried out directly on the beads containing nascent RNA using the iScript cDNA
302 synthesis kit. qPCR was processed as described in the RT-qPCR protocol. To quantify mRNA
303 and pre-mRNA, absolute amounts of RNA were estimated from standard curves. To assess
304 maturation from pre-mRNA to mRNA, mRNA expression level at each time point was divided by
305 pre-mRNA expression at 30min HS. In both analysis, mRNA and pre-mRNA expression
306 amounts were quantified relative to EU labeled *pmp-3* amounts.
307
308 **SUBCELLULAR FRACTIONATION**
309 Subcellular fractionation was performed with ~700 day-one adults per condition synchronized
310 through bleach hatching method. Worms were harvested in 1.5 ml tube with nuclease free
311 water, pelleted and snap-frozen in liquid nitrogen. Frozen pellet was washed with 500 µl
312 hypotonic buffer (15 mM HEPES/KOH (pH7.5), 10 mM KCl, 5 mM MgCl2, 0.1 mM EDTA, 350
313 mM Sucrose). Worms were resuspended in 100 µl hypotonic buffer supplemented with 1 mM
314 DTT, 1x PIC and 0.01U/µl SUPERase-In RNase inhibitor and homogenized by pestle (SP Bel-
315 Art ; Cat #F19923-0001). To remove worms' bodies and debris, homogenates were centrifuged
316 at 500 xg at 4°C for 5 mins, and supernatant was transferred to a new 1.5 ml tube. The
317 supernatant was then centrifuged at 4,000 xg at 4°C for 5 mins to collect nucleic (pellet) fraction.
318 The nuclei pellet was washed three times with 200 µl hypotonic buffer. After last washing, the
319 pellet was resuspended in 120 µl nucleus lysis buffer (50 mM Tris (pH7.5), 140 mM NaCl, 1.5
320 mM MgCl2, 0.5% (w/v) NP-40) supplemented with 1 mM DTT, 1x PIC and 0.01U/µl SUPERase-
321 In RNase inhibitor, and incubated in ice for 20 mins. 20 µl of sample was aliquoted to a 1.5 ml

322 tube labelled as "input", and the remaining samples were centrifuged at 20,000 xg at 4°C for 10
323 mins. The supernatant was transferred to a 1.5 ml tube labelled as "nucleoplasm". The pellet
324 was resuspended in 100 µl high salt solution (10 mM Tris (pH7.5), 700 mM NaCl) supplemented
325 with 1 mM DTT, 1x PIC and 0.01U/µl SUPERase-In RNase inhibitor, and incubated in ice for 20
326 mins, and centrifuged at 20,000 xg at 4°C for 5 mins. The supernatant was transferred to a 1.5
327 ml tube labelled as "Chromatin". The RNA in each sample was isolated using Trizol, and *hsp*
328 gene expression level was measured as described in the RT-qPCR protocol. The results of
329 experiments were presented as percentage input values.
330
331 This method of extraction did result in the loss of some nuclei. Nevertheless, the nuclei
332 obtained were 'clean' and not contaminated with cytoplasmic fractions, confirmed by conducting
333 a Western blot and probing for tubulin.
334
335 **EMBRYO HATCH RATE**
336 Embryo hatch rate was assessed using 2-5 day-one adult worms, which laid eggs for different
337 durations following NHS or 30min HS, as described previously[20] . After removing mothers,
338 embryos were counted and incubated at 20°C. The number of live progenies were scored after
339 72 hrs. For RNAi experiment, mothers were prepared by transferring them to RNAi plates at L4-
340 stage and allowed to lay eggs for 12 hrs after treatment.
341
342 **WESTERN BLOT**
343 Worm lysates were prepared by boiling samples in Laemmli sample buffer (Bio-Rad; Cat
344 #1610737) with β-mercaptoethanol. For ubiquitinylated protein analysis, about 150 worms were
345 prepared as described in the RNAi protocol. The worms were collected, snap frozen, and lysed
346 by boiling and grinding using a pestle. Lysates were separated on SDS-PAGE (HSP-70: 10%,
347 Ubiquitinylated protein: 12%) and transferred onto nitrocellulose membrane (Bio-Rad; Cat

348 #1620115). Membranes were blocked at RT for 1 hr in Odyssey Blocking Buffer (LI-COR; Cat
349 #927-50000), incubated overnight at 4°C with primary antibodies, and then with IRdye goat anti-
350 mouse IgG 800CW (1:10,000; LI-COR; Cat #926-32210) at RT for 2 hrs. Imaging was
351 performed using the LI-COR Odyssey Infrared System and analyzed with Image Studio
352 software.
353
354 To detect HSP-70 levels, mouse anti-FLAG M2 (1:1000; Sigma-Aldrich; Cat #F3165-1MG) was
355 used to detect HSP-70::FLAG in strains where endogenous *hsp-70* (C12C8.1) was tagged with
356 CRISPR/Cas9. Mouse anti-Ubiquitinylated proteins, clone FK2 (1:1000; Sigma-Aldrich; Cat #04-
357 263), was used to detect ubiquitinylated proteins. For tubulin detection as a loading control,
358 mouse anti-tubulin, clone AA4.3 (1:1000; DSHB; Cat #AB_579793) was used.
359
360 **SMALL RNA INJECTION AND RECOVERY ASSAY**
361 Small RNA was prepared from total RNA extracted from
362 (i) Wild-type animals worms subjected to 30 min HS
363 (ii) *prde-1* animals subjected to 30 min HS
364 Small RNAs were fractionated using the Mirvana miRNA Isolation Kit. The small RNA was then
365 injected at a concentration of 50 ng/µl. Following injection, worms were recovered at 20°C for 2
366 hrs and subsequently maintained under non heat shock conditions (NHS) or subjected to 30
367 mins heat shock at 34°C. Worms were collected in 1x PBS after 6 hrs incubation at 20°C and
368 used for *F44E5.4/.5* mRNA FISH experiment. For RT-qPCR analysis, worms were collected
369 immediately in Trizol, and their RNA harvested as described above.
370
371 **ANALYSIS OF mRNA VARIANTS**
372 To assess whether the loss of piRNAs led to increased transcript errors, we devised a method to
373 identify sequences of individual mRNA molecules prior to the possible incorporation of errors

374 due to PCR amplification. RNA extracted from 3 biological repeats of: wild type *C. elegans* at 30
375 minutes at 34ºC, and *prde-1* at 30 minutes at 34ºC were used. mRNAs were tagged with UMIs
376 using the **SMART-Seq® Total RNA Pico Input with UMIs (ZapR™ Mammalian)**. The UMIs
377 were attached to mRNAs during the first strand-cDNA synthesis, prior to PCR amplification.
378 Subsequently, mRNAs were PCR amplified with 3 cycles of amplification for the initial library
379 PCR and 12 cycles of amplification for the enrichment PCR. Sequencing was performed on the
380 Novaseq 6000; the number paired-end reads sequenced were in the range of 50 million-
381 80million, with a read size of 100 bp.
382
383 Next, data was pre-processed using a modified version of the RNA with UMIs v1.0.16 pipeline[24]
384 and a modified version of the GATK Best Practice: RNA-seq Variant Calling Workflow using the
385 tools from gatk (v4.6.1.0) and Picard (v3.3.0).
386
387 The complete list of relevant tools, and the custom script used are available on github
388 (https://github.com/Prahlad-Lab/umi_celegans_analysis_consensus)
389 DOI 10.5281/zenodo.17873233.
390
391 The fastq.gz files required to run this analysis pipeline are available through the European
392 Nucleotide Archive (ENA) at EMBL-EBI under accession
393 number PRJEB101605 (https://www.ebi.ac.uk/ena/browser/view/PRJEB101605).
394
395 FastQC [8] was used to check the quality of the FASTQ paired-end reads. The FASTQ files were
396 converted to unmapped bam (uBAM) using gatk FastqToSam tool. Unique molecular identifiers
397 (UMI) were extracted using fgbio ExtractUmifromBam. The UMI were extracted using the
398 parameters indicated in the SMART-Seq® Total RNA Pico Input with UMIs (ZapR™

399 Mammalian) kit, the SMART UMI Adapter from read2 was removed by trimming reads a total of
400 12 nucleotides: “8 nt UMIs + 3 nt UMI linker + 3 nt”. The quality of the uBAM file was measured
401 again with FastQC[8].
402
403 Reads were aligned to genome with STAR[25] (v 2.7.11b) using the *Caenorhabditis elegans*
404 genomic reference and annotation (ENSEMBL WBcel235 version 114)[26]. Per-Sample two pass-
405 mapping was enabled using the option -twopassMode Basic. The main output was an unsorted
406 BAM that included unmapped reads, --outSAMtype was set to "BAM Unsorted" and --
407 outSAMunmapped was set to "Within".
408
409 ***UMI Grouping and Consensus Generation***
410 Following alignment, BAM files were sorted by coordinating with Picard SortSam tool, then
411 merged with unaligned Bam file to get the UMI tags. **fgbio GroupReadsByUmi** was used to
412 create subgroups (families) based on their position, UMI, and, the parameters --strategy
413 Adjacency --edits 1 and --family-size-histogram were used to correct sequencing errors within
414 UMIs themselves and output the family sizes. Around 70-80% of the reads in all the replicates
415 were Family size =1, as shown in the plot (Method Table 4).

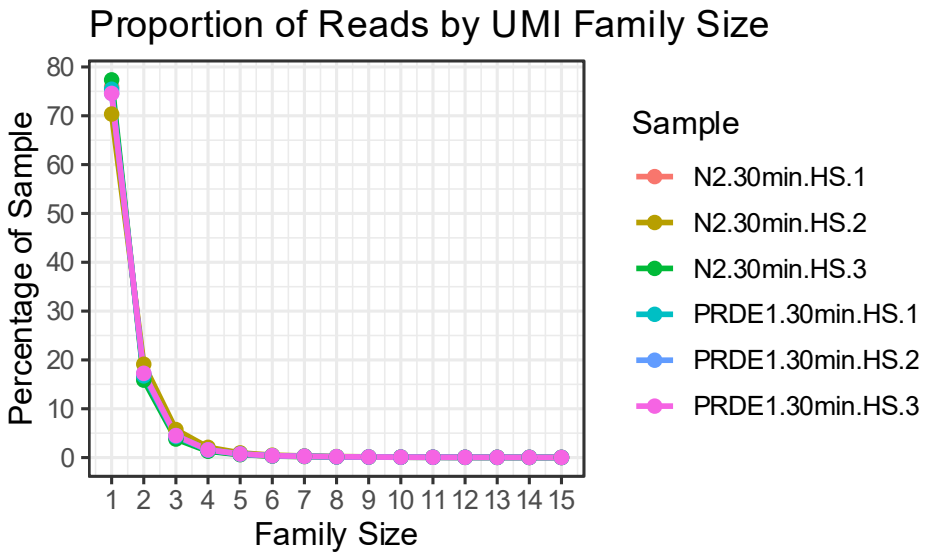

416

The different families were collapsed into single consensus reads by using fgbio CallMolecularConsensusReads. Families of size 1 were preserved using the parameter --min-reads 1. The consensus reads were mapped again to the WBcel235genome using STAR and merged again to unmapped BAM to get UMI tags.

Following the GATK best practices for RNA-seq Variants, BAM files were processed with gatk SplitNCigarReads to split the reads with “N” in their cigar. To filter out DNA variants, a recalibration model was built with gatk BaseRecalibrator. The resulting model was applied to the consensus BAM files with gatk ApplyBQSR to obtain the BSQR BAM.

Pileup Generation and analysis

A pileup of the BSQR BAM was generated with bcftools mpileup using the parameter -d 1000000 to get keep the reads at all loci. **To increase confidence that we were detecting mRNA variants, and not stochastic nucleotide changes we:**

i. analyzed only regions that had generated over 10 reads (i.e. at least 10 mRNAs corresponded to the region to identify the ones which were different). The pileup file was analyzed with a custom python script to filter the regions with total depth <=10 and count the proportion of alternative reads and reference reads.

ii. Excluded regions where “Alternative Read/Total Reads =1.0” or “0.5”. This was used to exclude possible homozygous or heterozygous SNPs with frequencies of 1 or 0.5, respectively, although this does not account for differences in expression from the different alleles.

A custom R script was used to generate tables with the statistics of the Total Number of “mistakes”, the Distribution of the Alternative Reads/Reference reads, a Kolmogorov-Smirnov

442 Test was used to compare the distributions. GO analysis of the genes with more mismatches in
443 PRDE1 than in N2 was performed.
444
445 ***Variant Call and Analysis***
446 HaplotypeCaller was used with the BSQR BAM to call variants and output VCF file. SnpEff [28]
447 was used to annotate the vcf with the SnpEff wbcel235 internal annotation. A custom R script
448 was used to read the VCF and filter the variants with total dept < =10, and SnpEFF Functional
449 Impact type of "Modifier". Variant Sites with a Ratio of Alternative Read/Total Reads =1.0were
450 excluded to remove potential genomic Variants. The following were calculated:
451 i. Transcription error rate: Ratio of Alternative Read/Total Reads
452 ii. Deleterious Variant Rates**:** Ratio Deleterious Variants/Total Reads
453 iii. Mismatch Error rate: change in nucleotides type.
454 iv. Two sample t-test was used to determine if there was statistical difference between
455 N2 and PRDE1 samples, with p-value,< 0.05 considered significant.
456
457 **STATISTICAL ANALYSIS**
458 **Statistical analysis (RNA-sequencing data):**
459 Anova with posthoc Tukey HSD was conducted to compare distribution of Gene Length in the
460 Differential Expressed Genes, with adjusted p-value <0.05 was considered significant. Wilcoxon
461 test was used to compare the expression of the piRNAs, difference between the means was
462 considered significant if the p-value <0.05. Hypergeometric test was done using the phyper
463 function in R[29], overlap was considered significant if p-value <0.05. Pearson's Chi-squared test
464 with Yates' correction was used to determine if the number of up- or down-regulated splicing
465 events during heat shock differed between the N2 and PRDE1 strains (p-value <0.05). All the
466 statistical analyses were done in R[29]. Kolmogorov–Smirnov test was used to compare the
467 probability distributions of mRNA error rates in the pileup analysis.

468 **Statistical analysis (qPCR data and phenotypes):**

469 The data were analyzed by using Student t-test (two-tailed unpaired t-test) or 2 way-ANOVA

470 (Fisher's LSD test; GraphPad Prism software) as described in respective figure legends. P

471 values are indicated as follows: $*p < 0.05$; $**p < 0.01$; $***p < 0.001$.

472 **Statistical analysis (other):**

473 The statistical analyses for the remaining datasets are indicated in the Figure Legends.

474

475 **DATA AVAILABILITY**

476 The data for this study have been deposited in the European Nucleotide Archive (ENA) at

477 EMBL-EBI under accession numbers PRJEB101605

478 (https://www.ebi.ac.uk/ena/browser/view/PRJEB101605), PRJEB101594

479 (https://www.ebi.ac.uk/ena/browser/view/PRJEB101594),

480 PRJEB101181(https://www.ebi.ac.uk/ena/browser/view/PRJEB101181) .

481

482

REFERENCES

1 Das, S. *et al.* Serotonin signaling by maternal neurons upon stress ensures progeny survival. *Elife* **9** (2020). https://doi.org:10.7554/eLife.55246

2 Tate, A. J., Brown, K. C. & Montgomery, T. A. tiny-count: a counting tool for hierarchical classification and quantification of small RNA-seq reads with single-nucleotide precision. *Bioinformatics Advances* **3** (2023). https://doi.org:10.1093/bioadv/vbad065

3 Chen, S., Zhou, Y., Chen, Y. & Gu, J. fastp: an ultra-fast all-in-one FASTQ preprocessor. *Bioinformatics* **34**, i884-i890 (2018). https://doi.org:10.1093/bioinformatics/bty560

4 Langmead, B., Trapnell, C., Pop, M. & Salzberg, S. L. Ultrafast and memory-efficient alignment of short DNA sequences to the human genome. *Genome Biol* **10**, R25 (2009). https://doi.org:10.1186/gb-2009-10-3-r25

5 Lawrence, M., Gentleman, R. & Carey, V. rtracklayer: an R package for interfacing with genome browsers. *Bioinformatics* **25**, 1841-1842 (2009). https://doi.org:10.1093/bioinformatics/btp328

6 Benjamini, Y. & Hochberg, Y. Controlling the False Discovery Rate: A Practical and Powerful Approach to Multiple Testing. *Journal of the Royal Statistical Society: Series B (Methodological)* **57**, 289-300 (1995). https://doi.org:https://doi.org/10.1111/j.2517-6161.1995.tb02031.x

7 Di Tommaso, P. *et al.* Nextflow enables reproducible computational workflows. *Nat Biotechnol* **35**, 316-319 (2017). https://doi.org:10.1038/nbt.3820

8 (2015).

9 Bolger, A. M., Lohse, M. & Usadel, B. Trimmomatic: a flexible trimmer for Illumina sequence data. *Bioinformatics* **30**, 2114-2120 (2014). https://doi.org:10.1093/bioinformatics/btu170

10 Cingolani, P. *et al.* A program for annotating and predicting the effects of single nucleotide polymorphisms, SnpEff: SNPs in the genome of Drosophila melanogaster strain w1118; iso-2; iso-3. *Fly (Austin)* **6**, 80-92 (2012). https://doi.org:10.4161/fly.19695

11 Garcia-Alcalde, F. *et al.* Qualimap: evaluating next-generation sequencing alignment data. *Bioinformatics* **28**, 2678-2679 (2012). https://doi.org:10.1093/bioinformatics/bts503

12 Wang, L., Wang, S. & Li, W. RSeQC: quality control of RNA-seq experiments. *Bioinformatics* **28**, 2184-2185 (2012). https://doi.org:10.1093/bioinformatics/bts356

13 Trincado, J. L. *et al.* SUPPA2: fast, accurate, and uncertainty-aware differential splicing analysis across multiple conditions. *Genome Biol* **19**, 40 (2018). https://doi.org:10.1186/s13059-018-1417-1

14 Wu, T. *et al.* clusterProfiler 4.0: A universal enrichment tool for interpreting omics data. *Innovation (Camb)* **2**, 100141 (2021). https://doi.org:10.1016/j.xinn.2021.100141

15 Yu, G., Wang, L. G., Han, Y. & He, Q. Y. clusterProfiler: an R package for comparing biological themes among gene clusters. *OMICS* **16**, 284-287 (2012). https://doi.org:10.1089/omi.2011.0118

16 Carlson, M. (2023).

17 Ramirez, F. *et al.* deepTools2: a next generation web server for deep-sequencing data analysis. *Nucleic Acids Res* **44**, W160-165 (2016). https://doi.org:10.1093/nar/gkw257

18 {eulerr}: Area-Proportional Euler and Venn Diagrams with Ellipses v. R package version 7.0.2 (2024).

19 Wickham, H. ggplot2: Elegant Graphics for Data Analysis. (2016).

20 Das, S., Min, S. & Prahlad, V. Gene bookmarking by the heat shock transcription factor programs the insulin-like signaling pathway. *Mol Cell* **81**, 4843-4860 e4848 (2021). https://doi.org:10.1016/j.molcel.2021.09.022

21 Kamath, R. S. & Ahringer, J. Genome-wide RNAi screening in Caenorhabditis elegans. *Methods* **30**, 313-321 (2003). https://doi.org:10.1016/s1046-2023(03)00050-1

533 22 Muir, V. S., Gasch, A. P. & Anderson, P. The Substrates of Nonsense-Mediated mRNA
534 Decay in Caenorhabditis elegans. *G3 (Bethesda)* **8**, 195-205 (2018).
535 https://doi.org:10.1534/g3.117.300254
536 23 Das, P. P. *et al.* Piwi and piRNAs act upstream of an endogenous siRNA pathway to
537 suppress Tc3 transposon mobility in the Caenorhabditis elegans germline. *Mol Cell* **31**,
538 79-90 (2008). https://doi.org:10.1016/j.molcel.2008.06.003
539 24 Degatano, K. *et al.* Warp Analysis Research Pipelines: Cloud-optimized workflows for
540 biological data processing and reproducible analysis. *Bioinformatics* (2025).
541 https://doi.org:10.1093/bioinformatics/btaf494
542 25 Dobin, A. *et al.* STAR: ultrafast universal RNA-seq aligner. *Bioinformatics* **29**, 15-21
543 (2013). https://doi.org:10.1093/bioinformatics/bts635
544 26 Sternberg, P. W. *et al.* WormBase 2024: status and transitioning to Alliance
545 infrastructure. *Genetics* **227** (2024). https://doi.org:10.1093/genetics/iyae050
546 27 Crombie, T. A. *et al.* CaeNDR, the Caenorhabditis Natural Diversity Resource. *Nucleic*
547 *Acids Res* **52**, D850-D858 (2024). https://doi.org:10.1093/nar/gkad887
548 28 Cingolani, P. Variant Annotation and Functional Prediction: SnpEff. *Methods Mol Biol*
549 **2493**, 289-314 (2022). https://doi.org:10.1007/978-1-0716-2293-3_19
550 29 R: A Language and Environment for Statistical Computing (2023).
551

Table 1. Strain information

Strain name	Genotype		Source	Note
N2	Bristol N2; Wild-type		CGC	
sx2499	*prde-1(mj207) V*		CGC	
PS3551	*hsf-1 (sy441) I*		CGC	
FLAG::HSF-1	*3X flag::hsf-1 I*	CRISPR /Cas-9	Prahlad Lab	
FLAG::HSF-1 (*sy441*)	*3X flag::hsf-1(sy441) I*	CRISPR /Cas-9	Prahlad Lab	
WM274	*prg-1(tm872) I; neSi14 [FLAG::prg-1 + Cbr-unc-119(+)] II; unc-119(ed3) III.*		CGC	
JDW10	*wrdSi3 [sun-1p::TIR1::F2A::mTagBFP2::AID*::NLS ::tbb-2 3'UTR] II*		CGC	
VP27	*prde-1::AID (syb7464) V*	CRISPR /Cas-9	Prahlad Lab /SunyBiotech	
JDW10 ;VP27	*wrdSi3 [sun-1p::TIR1::F2A::mTagBFP2::AID*::NLS ::tbb-2 3'UTR] II; prde-1::AID (syb7464) V*	Cross	Prahlad Lab	JDW10 was selecte d by picking BFP positive worms
VP01	*C12C8.1::FLAG (syb2141) I*	CRISPR /Cas-9	Prahlad Lab / SunyBiotech	
VP01; sx2499	*C12C8.1::FLAG (syb2141) I; prde-1(mj207) V*	Cross	Prahlad Lab	

Table 2. Primer information

Experiments	Name	Forward	Reverse
Genotype	VP01	CTCAAGCTGATATTGATAGA	AGCTAATTGTACAGAGAAAA
	VP27 (Outside AID insertion)	CGTCAAATATGTTGCGCATT	AAAATTCATTCCGCAGCAAC
	VP27 (Inside AID insertion)	GGTTTCCTGCCAAAAATCAA	AAAATTCATTCCGCAGCAAC
	sx2499	GAAATCGCAAAGGACACGAT	CGGCTTGTCACACACAAGAT
Multiple Experiments	*hsp-70 (C12C8.1)* pre-mRNA	TTTATTTTCCGTTTTCAGGTTGA	CCACGTAGGAAGGCGTAGTC
	hsp-70 (C12C8.1) mRNA	TTGGTTGGGGGATCAACTCG	GAGCAGTTGAGGTCCTTCCC
	F44E5.4/.5 pre-mRNA	CGGTACTACGTACTCGTGTGTTG	TGTTATTAAAATTGAAAATGCCAAA
	F44E5.4/.5 mRNA	CTATCAGAATGGAAAGGTTGAG	TCTTTCCGTATCTGTGAATGCC
	hsp-16.11 pre-mRNA	TGAATCTTCTGAGGTAAGTAACACG	GCTTGAACTGCGAGACATTG
	hsp-16.11 mRNA	CTCCATCTGAATCTTCTGAGATTGT	TCTGGCTTGAACTGCGAGAC
	pmp-3 mRNA	TAGAGTCAAGGGTCGCAGTG	ATCGGCACCAAGGAAACTGG
PCR for generating Standard Curve	*hsp-70 (C12C8.1)* (cDNA)	CCCGTTGTTGAGGTTGAAGT	CGGCAGCTGATACATTGAGA
	hsp-70 (C12C8.1) (gDNA)	ACGTACTCATGTGTCGGTAT	CGGCAGCTGATACATTGAGA
	F44E5.4/.5 (cDNA)	CTATCAGAATGGAAAGGTTGAG	TCACAAGCAGTTCGGAGACG
	F44E5.4/.5 (gDNA)	TAAAAGGGCTGGGATTCGGG	TCACAAGCAGTTCGGAGACG
	pmp-3 (cDNA)	TGGAGACAGTGGATGTGGAA	GAAAGAACTGTATCGGCACCA
RIP-RT-qPCR	*bath-45* mRNA	ACGATAGGCCTTTTCCAATG	GAGCTGCCTTTTCCAAATTC
ChIP-qPCR	*hsp-70 (C12C8.1)* TSS	ACGTACTCATGTGTCGGTAT	TCTTCTTCCAGTTTACATAATCCT
	hsp-70 (C12C8.1) End	ACAATTCGCAATGAGAAGGGACG	GCATCTTCTGCTGATAACAGTGATC

	F44E5.4/.5 TSS	TAAAAGGGCTGGGATTCGGG	ACCGAGGTCGATACCAATAGC
	F44E5.4/.5 End	TTGATGAAACACTTCGTTGGTTGG	TCCAGCAGTTCCAGGATTTC
RT-qPCR	*T08G5.11*	CGATCAAGAAGGCGGAATCC	TCAACTCGAGACTGCCACAC
	H27M09.6	GCGATCACAAAGGCGGAATC	TCAACTCGAGACTGCCACAC
	F08H9.10	ATCAAGAAGGCGGAATCCCC	TCAACTCGAGACTGCCACAT
	sup-6	TGATCATGAAGACGGAATCCCC	TCAACTCGAGACTGCCACAC
	sup-39	GCCTACCCATTGCACTTTTGG	GCAGCCCCGATACGCAAAA
	eft-3	ACTTGATCTACAAGTGCGGAGGA	AAAGATCCCTTACCCATCTCCTG
	linc-9	AAGACTACGCCCTGGAC	CTTCTCGAATTGTAGTGGTCG
	nhr-109	GCAGGGAATGAAGGATTATACG	AATGGAATGTAGGAGTTGCG
	B0495.8	GAGTATGTCCTCACGATATGG	GTTTACGATACGCTCGCAG
	F53B2.8	GGATTTGGGAGATGCTATGAG	CGTACCCTTTTCTGGTGTTTC
	Y39B6A.21	GCCCTGGATAGTGTTAATTGTG	GCTGTCTTTGTCTCCGAAAAG

* Genotyping of sx2499 mutant was verified through digestion with MuCI.

Table 3. Primer information (small RNA)

Experiments	Name	Sequence	Targeting 22G RNA sequence
22G RNA FISH	*F44E5.4/.5* 22G RNA	ATCAGTTTGTCAATCAATTCTC	GAGAATTGATTGACAAACTGAT
sRNA RT-qPCR	*hsp-70 (C12C8.1)* **Stem-loop (SL)**	CTCAACTGGTGTCGTGGAGTCGGCAATTCAGTTGAGTCTATTCG	GCACGTGTGATTTTCGAATAGA
	hsp-70 (C12C8.1) 22G RNA **Forward**	ACACTCCAGCTGGGGCACGTGTGATTTTCG	
	F44E5.4/.5 **Stem-loop (SL)**	CTCAACTGGTGTCGTGGAGTCGGCAATTCAGTTGAGATCAGTTT	GAGAATTGATTGACAAACTGAT
	F44E5.4/.5 22G RNA **Forward**	ACACTCCAGCTGGGGAGAATTGATTGACAA	
	universal **Reverse** primer	CTCAAGTGTCGTGGAGTCGGCAA	
Synthetic RNA	21ur-2348	UGAUGUCCCAUGUCGCAAUUC	

* synthetic 21ur-2348 RNA has 5' phosphorylation at 5' end and 2' O-methyl bases at 3' end

Table 4. UMI Family Size

SAMPLE	FAMILY SIZE	NUMBER OF UMI-FAMILIES	PERCENTAGE OF FAMILIES
N2.30MIN.HS.1	1	24524361	75.959
N2.30MIN.HS.1	2	5400148	16.7258
N2.30MIN.HS.1	3	1336034	4.1381
N2.30MIN.HS.1	4	451271	1.3977
N2.30MIN.HS.1	5	203684	0.6309
N2.30MIN.HS.1	6	106590	0.3301
N2.30MIN.HS.1	7	70936	0.2197
N2.30MIN.HS.1	8	43942	0.1361
N2.30MIN.HS.1	9	31135	0.0964
N2.30MIN.HS.1	10	22472	0.0696
N2.30MIN.HS.1	11	16931	0.0524
N2.30MIN.HS.1	12	12091	0.0374
N2.30MIN.HS.1	13	10270	0.0318
N2.30MIN.HS.1	14	7700	0.0238
N2.30MIN.HS.1	15	6294	0.0195
N2.30MIN.HS.2	1	30086473	70.356
N2.30MIN.HS.2	2	8174687	19.1162
N2.30MIN.HS.2	3	2454899	5.7407
N2.30MIN.HS.2	4	896515	2.0965
N2.30MIN.HS.2	5	410860	0.9608
N2.30MIN.HS.2	6	208172	0.4868
N2.30MIN.HS.2	7	141249	0.3303
N2.30MIN.HS.2	8	87246	0.204
N2.30MIN.HS.2	9	62244	0.1456
N2.30MIN.HS.2	10	45576	0.1066
N2.30MIN.HS.2	11	34216	0.08
N2.30MIN.HS.2	12	24578	0.0575
N2.30MIN.HS.2	13	21183	0.0495
N2.30MIN.HS.2	14	15921	0.0372
N2.30MIN.HS.2	15	12649	0.0296
N2.30MIN.HS.3	1	25262426	77.3577
N2.30MIN.HS.3	2	5177514	15.8544
N2.30MIN.HS.3	3	1237052	3.7881
N2.30MIN.HS.3	4	423263	1.2961
N2.30MIN.HS.3	5	195074	0.5973
N2.30MIN.HS.3	6	101639	0.3112
N2.30MIN.HS.3	7	69452	0.2127
N2.30MIN.HS.3	8	43029	0.1318
N2.30MIN.HS.3	9	30368	0.093

N2.30MIN.HS.3	10	22085	0.0676
N2.30MIN.HS.3	11	16736	0.0512
N2.30MIN.HS.3	12	11993	0.0367
N2.30MIN.HS.3	13	10153	0.0311
N2.30MIN.HS.3	14	7569	0.0232
N2.30MIN.HS.3	15	6034	0.0185
PRDE1.30MIN.HS.1	1	28484889	75.4403
PRDE1.30MIN.HS.1	2	6316795	16.7296
PRDE1.30MIN.HS.1	3	1615033	4.2773
PRDE1.30MIN.HS.1	4	566822	1.5012
PRDE1.30MIN.HS.1	5	266046	0.7046
PRDE1.30MIN.HS.1	6	139724	0.37
PRDE1.30MIN.HS.1	7	96951	0.2568
PRDE1.30MIN.HS.1	8	59486	0.1575
PRDE1.30MIN.HS.1	9	42911	0.1136
PRDE1.30MIN.HS.1	10	31353	0.083
PRDE1.30MIN.HS.1	11	23826	0.0631
PRDE1.30MIN.HS.1	12	16649	0.0441
PRDE1.30MIN.HS.1	13	14570	0.0386
PRDE1.30MIN.HS.1	14	11210	0.0297
PRDE1.30MIN.HS.1	15	8782	0.0233
PRDE1.30MIN.HS.2	1	28896617	74.5928
PRDE1.30MIN.HS.2	2	6660140	17.1923
PRDE1.30MIN.HS.2	3	1744353	4.5028
PRDE1.30MIN.HS.2	4	613302	1.5832
PRDE1.30MIN.HS.2	5	285714	0.7375
PRDE1.30MIN.HS.2	6	148717	0.3839
PRDE1.30MIN.HS.2	7	102995	0.2659
PRDE1.30MIN.HS.2	8	63467	0.1638
PRDE1.30MIN.HS.2	9	45498	0.1174
PRDE1.30MIN.HS.2	10	33617	0.0868
PRDE1.30MIN.HS.2	11	25055	0.0647
PRDE1.30MIN.HS.2	12	17947	0.0463
PRDE1.30MIN.HS.2	13	15305	0.0395
PRDE1.30MIN.HS.2	14	11683	0.0302
PRDE1.30MIN.HS.2	15	9226	0.0238
PRDE1.30MIN.HS.3	1	28795499	74.5599
PRDE1.30MIN.HS.3	2	6667426	17.2639
PRDE1.30MIN.HS.3	3	1736294	4.4958
PRDE1.30MIN.HS.3	4	605894	1.5688
PRDE1.30MIN.HS.3	5	280303	0.7258
PRDE1.30MIN.HS.3	6	145531	0.3768
PRDE1.30MIN.HS.3	7	101463	0.2627

PRDE1.30MIN.HS.3	8	62804	0.1626
PRDE1.30MIN.HS.3	9	44520	0.1153
PRDE1.30MIN.HS.3	10	33263	0.0861
PRDE1.30MIN.HS.3	11	25169	0.0652
PRDE1.30MIN.HS.3	12	17905	0.0464
PRDE1.30MIN.HS.3	13	15608	0.0404
PRDE1.30MIN.HS.3	14	11845	0.0307
PRDE1.30MIN.HS.3	15	9208	0.0238